Report no. changed (Mar 2006): SM-265-UU

SACLANTCEN MEMORANDUM
serial no.: SM-265

SACLANT UNDERSEA
RESEARCH CENTRE

MEMORANDUM

Ocean currents in the Iceland–Faeroe area, measured by a bottom-mounted ADCP

H.-H. Essen

December 1992

Page count for SM-265 (excluding Covers and Data Sheet)

Pages	Total
i–vi	6
1–43	43
	49

SACLANT Undersea Research Centre
Viale San Bartolomeo 400
19138 San Bartolomeo (SP), Italy

tel: 0187 540 111
fax: 0187 524 600
telex: 271148 SACENT I

NORTH ATLANTIC TREATY ORGANIZATION

SACLANTCEN SM-265

Ocean currents in the Iceland–Faeroe area, measured by a bottom-mounted ADCP

H.-H. Essen

The content of this document pertains to work performed under Project 23 of the SACLANTCEN Programme of Work. The document has been approved for release by The Director, SACLANTCEN.

Issued by:
Underwater Research Division

H. Urban
Division Chief

intentionally blank page

SACLANTCEN SM-265

Ocean currents in the Iceland–Faeroe area, measured by a bottom-mounted ADCP

H.-H. Essen

Executive Summary: The performance of sonar systems depends on the spatial sound-speed structure within the ocean, which may change considerably with time. The sound-speed changes are mainly due to currents which are nearly always present. Currents, through their mass movement of water, may modify frontal structures or cause mixing in the upper layer of the ocean. Time scales of current variability of main interest for sonar performance extend from a few hours to some days.

Current measurements by means of a bottom-mounted acoustic doppler current profiler (ADCP) were carried out for 34 days in August 1990 and for 202 days from August 1991 to March 1992 in the Iceland–Faeroe area. This instrument measures horizontal current velocities as a function of depth. The main advantage over conventional current meters is the vertical coverage performed by the ADCP. Methods of time-series analysis have been applied in order to determine the dominant oceanic processes in the area under consideration, which are the semidiurnal barotropic tide, inertial motions and internal tides. Near-surface currents are highly correlated with winds.

Sound-velocity profiles can be measured at selected positions and times only. Future work will investigate their horizontal and temporal variability by making use of all data available. These are measured sound-velocity profiles, information on horizontal variability from satellite imagery and current measurements as presented in this memorandum.

intentionally blank page

SACLANTCEN SM-265

Ocean currents in the Iceland–Faeroe area, measured by a bottom-mounted ADCP

H.-H. Essen

Abstract: Horizontal currents as a function of depth, measured by a bottom-mounted acoustic doppler current profiler (ADCP) in the Iceland-Faeroe area have been analysed. Because of instrumental limitations it was expected that currents measured in the upper 15% of the water column would be contaminated by side-lobe reflections from the sea surface. Some evidence has been found that this effect is less important in the upper part of the contaminated layer.

The uncontaminated data are of high quality and cover about 75% of the water column. By means of least-squares methods, tidal currents have been extracted. The semidiurnal tide M2 is dominant, its barotropic portion has been estimated from vertically averaged currents. After removing the tides, the only significant variance peak left is for clockwise rotating currents around the inertial period. Vertical coherence between currents at different depth levels has been investigated and a decomposition into empirical orthogonal eigenfunctions (EOFs) has been performed.

A surprisingly high correlation has been found between low-pass filtered current velocities at the (contaminated) near-surface level and wind velocities from the wind archive of the UK Meteorological Office.

Keywords: bottom-mounted ADCP (acoustic doppler current profiler) ○ Iceland-Faeroe area ○ tides ○ inertial motions ○ winddriven currents

Contents

Acknowledgements: The ADCP data were collected and processed by the Ocean Engineering Department (OED) and the Applied Oceanography Group (AOG) at SACLANTCEN. Thanks go to the UK Meteorological Office for supplying the wind data.

1
Introduction

Project 23 explores possible applications of data remotely sensed by satellites. Satellite data have the advantage of covering highly extended areas of the ocean nearly synoptically, but the disadvantage of being restricted to the sea surface. For oceanographic and acoustic purposes, extension of satellite information to subsurface structures is required. With respect to sea-surface temperatures, as deduced from infrared radiometers, ship-borne surveys with towed thermistor chains yield some of the desired information. The observed structures include both spatial and temporal variability. Additional information on purely temporal variability may be obtained from current meters.

Mixing and advection of temperature structures are due to currents. In the Iceland–Faeroe area, these effects are of great importance. Unfortunately, no reliable current measurements are available for the upper 50 m of the ocean in this area. For this reason, data as obtained from a bottom-mounted acoustic doppler current profiler (ADCP) during 34 days in August 1990 and for 202 days from August 1991 to March 1992 are of great interest. The ADCP measures horizontal current velocities as a function of depth, by averaging over range bins of selected extension, 8 m for the 1990 mooring and 16 m for the 1991/92 mooring. Due to possible contamination by sidelobe reflections at the sea surface, data from the near-surface layer, extending to a depth of about 15% of the water depth, have to be considered with care. For the moorings under consideration this is about 60 m.

Methods of time-series analysis have been applied to the 1-hourly sampled horizontal current velocities. In ddition to oceanographic aspects, another purpose of this paper is to investigate the reliability of near-surface ADCP data. From geometric arguments (Sect. 2) it may be concluded that contamination by sidelobe reflections should decrease from a critical depth towards the sea surface. Confirmation for this assumption is found in the depth dependence of mean current velocities (Sect. 2) and M2 tidal ellipses (Sect. 3). Coherence spectra of currents from adjacent depth levels show similar features for all uncontaminated levels and also for the two levels below the sea surface, but much less coherence for levels just above the critical depth (Sect. 5). Another indication of the quality of near-surface ADCP data is their high correlation with winds, as obtained from the wind archive of the UK Meteorological Office (Sect. 7).

The main advantage of the ADCP over conventional current meters is the extended vertical coverage, which allows a more reliable estimation of barotropic currents. Barotropic transport is mainly parallel to depth contours (Sect. 2), and

the barotropic M2 tide appears to be very stable over the half-year period of the 1991/92 mooring (Sect. 3). Rotational variance spectra (Sect. 4) contain main peaks at tidal frequencies. After removing tides, a broad spectrum around the inertial period remains only for clockwise rotating currents, indicating the presence of inertial motions. Near-surface currents show different frequency dependencies at the high frequency tail of the spectrum. The reason for this finding is not understood.

Coherence spectra from currents at adjacent and distant depth horizons are presented in Sect. 5. Decomposition of the depth dependent current into vertical EOFs is performed in Sect. 6.

2 Data

A bottom-mounted ADCP (acoustic doppler current profiler) was deployed twice by SACLANTCEN in the Iceland–Faeroe area. During summer 1990 data were collected for a period of 817 h starting on Julian day 196/1990. The following mooring was operated for more than half a year, starting on Julian day 229/1991 and ending on 66/1992, covering a period of 4860 h. The data collected are both components of horizontal current velocity at equidistantly spaced depth horizons.

The ADCP operates by transmitting acoustic pulses and segmenting the backscattered echo into depth cells. Backscattering occurs within the water column from small particles drifting with the current, which cause a doppler-shift in the received signal. The measured doppler-shift allows the determination of the current component parallel to the acoustic beam. The ADCP uses a four beam configuration, the beams of which are orientated 30° off vertical and in 90° azimuthal increments. From the respective radial current velocities two-dimensional vectors are determined. A detailed decription of the ADCP is given by RD Instruments (1989).

Figure 1 shows the geometry of the ADCP as operated in the Iceland–Faeroe area, with the water depth refering to the summer 1990 mooring. The sketch shows two of the four acoustic main beams, pointing in opposite directions. Obviously, the components of current velocity used for computing the two-dimensional vector are taken from different positions, with distances increasing towards the sea surface. In order to obtain reliable current vectors it has to be assumed that the currents are homogeneous over this range.

Another important feature of the ADCP is also shown by the figure. In addition to the main lobe, some energy is transmitted to sidelobes at different angles. Due to the much lower intensity their contribution may be ignored in the case of volume scattering, but higher scattering strengths at the sea surface may cause contaminations of the signal in the case of simultaneous arrivals. Figure 1 shows that the main-lobe signal may be contaminated by sidelobe contributions in the upper $\sim 15\%$ of the total vertical range, which are about 60 m for the configuration shown. The dashed curve corresponds to the travel time of a sidelobe first touching the sea surface. It should be mentioned that surface scattering is highest in the case of specular reflection, which occurs from sea-wave slopes for a certain angle range around perpendicular incidence. Thus it may be expected that sidelobe contamination is highest at the depth indicated by the dashed line in the figure and decreases towards the surface, because contaminating sidelobes contain decreasing specularly reflected portions. In the data analysed, there is some evidence for this effect.

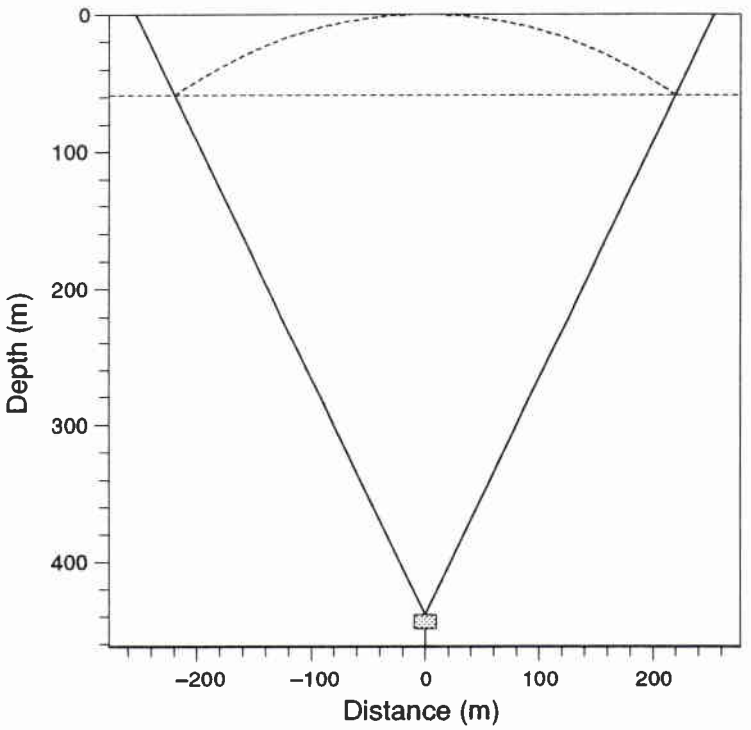

Figure 1 *Geometry of the bottom-mounted ADCP, installed at the Iceland–Faeroe Front in summer 1990. Solid lines represent two main beams 30° off the vertical. The dashed line marks the depth above which current velocities may be contaminated by surface-reflected sidelobes.*

The ADCP was operated at a frequency of 75 kHz. For the 1990 mooring a vertical resolution of 8 m was selected, yielding 52 horizons from 427 m to 19 m below the sea surface. The vertical resolution of the 1991/92 mooring was 16 m with 24 horizons from 376 m to 8 m. Depth resolution is obtained by segmenting the received backscattered signal, where the range gate duration is set to equal the length of the transmitted pulse. The current velocities determined represent weighted vertical averages within the range gates. Current velocities of adjacent depth cells are correlated by about 15%. Figure 2 shows the locations of the bottom-mounted ADCP during the two mooring periods together with the bathymetry. In summer 1990 the water depth at position P1 was 462 m and the tranducers were installed at 439 m, the respective values for the half-year mooring 1991/92 at position P2 were 417 m and 404 m.

The current velocities used for further analysis are averaged to 1-hour sampling rate. Figures 3a and 3b display the total length of vector time series from the two mooring periods at three different depths. East and north components of velocity are shown separately. Horizons closest to the bottom, just below the critical level of contamination and close to the surface are presented. For surface currents the

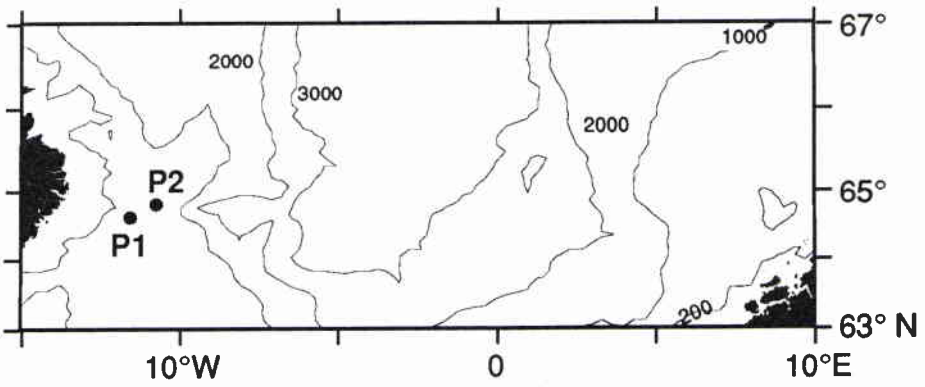

Figure 2 *Topography and bathymetry of the Iceland–Faeroe area, and positions of ADCP moorings 1990 (P1) and 1991/92 (P2). Depth contours are in metres.*

second uppermost horizon is shown, because data of the uppermost contain some spikes and may be contaminated by surface waves. Again, it should be mentioned that these current velocities may be contaminated by sidelobe reflections.

For further investigation time series of equal length of 810 h were constructed. For summer 1990, the period considered covers nearly the whole mooring time, while 6 distinct partial series are available from the half-year mooring of 1991/92. Figure 4 shows the depth dependence of currents by displaying the temporal averages of the east- and north-component and the rms values of the speed as a function of depth. In order to suppress tidal contributions to the means, the time series have been shortened to 808 h, which is about 65 times the dominant M2 period. Results from the 1990 mooring and from the first partial times series of the 1991 mooring (summer condition) and the last one (winter condition) are presented. The starting time of the series are indicated by the Julian day. The dashed lines mark the critical depth above which current velocities may be contaminated by sidelobe reflections at the sea surface, for which the predicted effect is an underestimation of speed. Indeed, this becomes visible in the rms values, which are minimal just above the critical depth. The rms-values contain an important contribution from tides and are relatively high and nearly constant for depths exceeding 60 m.

Table 1 contains vertically averaged mean velocities and variances for all partial time series available. The lengths of the series considered are again 808 h. Vertical averaging is performed from the deepest horizon recorded up to the critical depth of contamination, i.e. over about 75% of the water column, see Fig. 4. As the ADCP performs vertical averaging within the single depth horizons, the mean current velocities can be assumed to represent a good estimate of the barotropic velocity.

For the summer 1990 mooring the mean transport is mainly towards the southwest and follows the depth contours, see Fig. 2. For the sections of the 1991/92 mooring

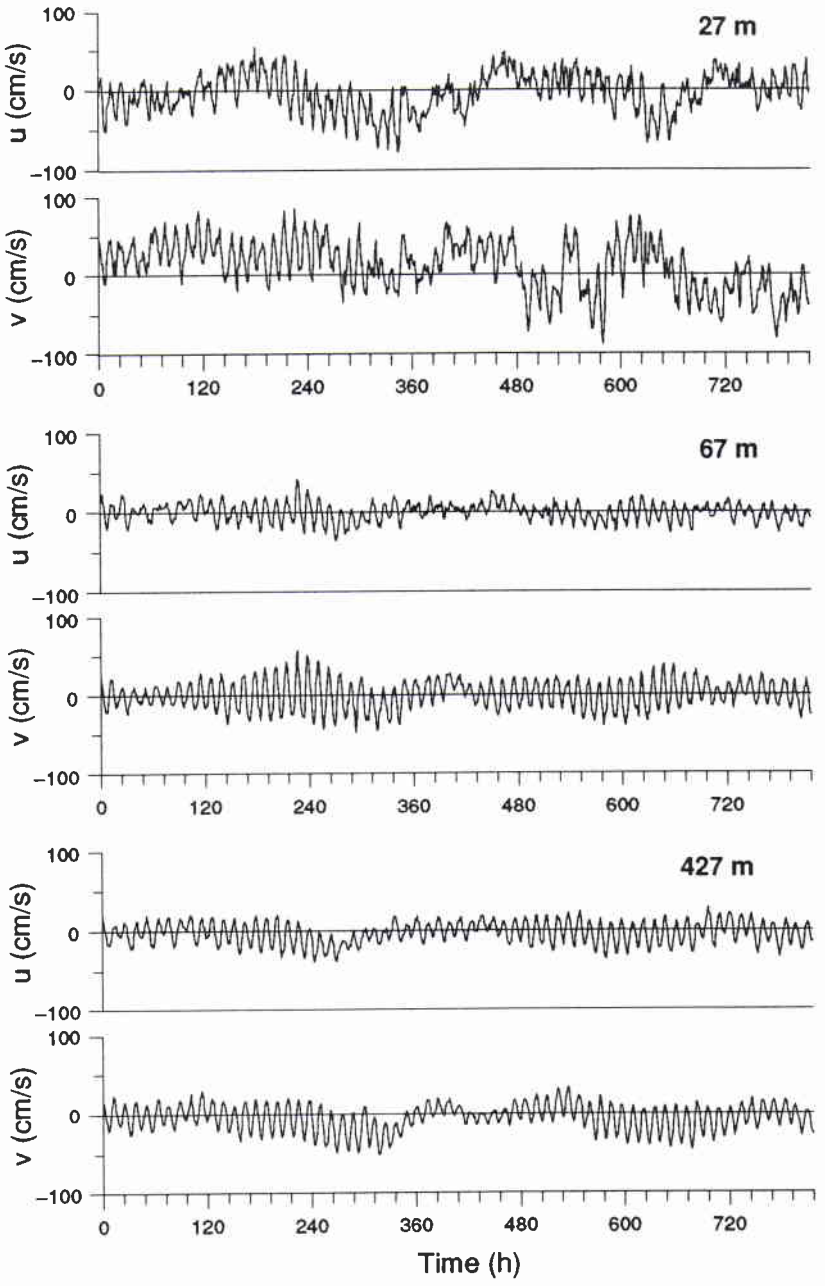

Figure 3a *Current velocities (u, v) from bottom-mounted ADCP, at three depth horizons from the 1990 mooring, starting on Julian day 196.00.*

there is some variation but the main direction is towards the northeast, i.e. opposite to the summer 1990 mooring.

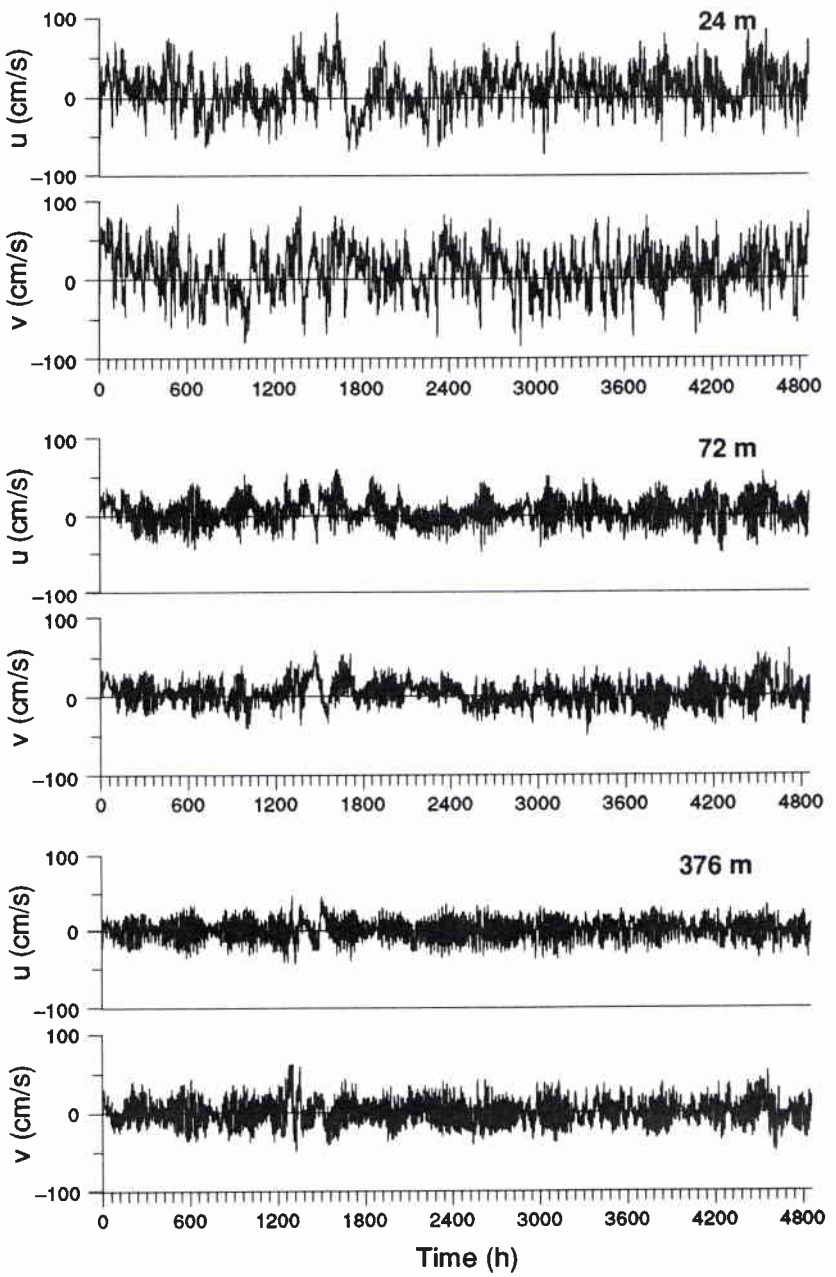

Figure 3b *Current velocities (u, v) from bottom-mounted ADCP, at three depth horizons from mooring 1991/92, starting on Julian day 229.00.*

Table 1 *Mean components of current velocity and rms value of speed from 808 h time series with starting time in Julian days.*

Year	1990	1991	1991	1991	1991	1991	1992
Day	196.00	229.00	262.75	296.50	330.25	364.00	32.75
u_{mean}	−2.7	1.9	4.9	1.5	1.4	2.3	1.6
v_{mean}	−4.8	2.8	4.4	5.1	−0.9	0.4	2.5
rms	21.7	19.8	23.8	20.1	20.7	19.3	20.8

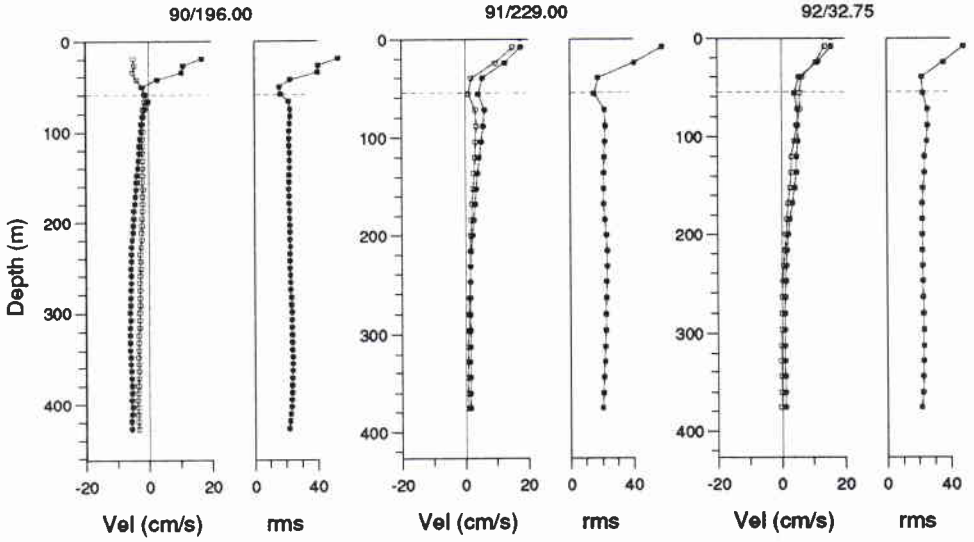

Figure 4 *Mean and rms current velocities as function of depth, from time series of 808 h duration: 1990 mooring (left panel), 1991/92 mooring, first (middle panel) and last (right panel) of 6 partial series, with starting time in terms of Julian day. Mean u (open circles) and v (filled circle) are displayed, the rms values contain the variance of both components. For the dashed lines see Fig. 1.*

3 Tides

A tidal analysis is carried out to determine the tidal parts of the current time series, and also to remove these parts for further investigation. For some analysis, such as evaluating rotational spectra, it is convenient to represent the two-dimensional current vector by a complex number

$$w = v + iu = U \exp(i\theta), \tag{3.1}$$

where v and u are the north- and east-component of current velocity, respectively, U is the speed and θ the direction counts counting clockwise from the north.

The tidal portion of a current time series may be described by the sum of a finite number L of tidal harmonics

$$w_T(t) = \sum_{l=1}^{L} w_l(t), \tag{3.2}$$

with each harmonic of circular frequency ω_l represented by a tidal ellipse

$$w_l(t) = \tfrac{1}{2} i[(A_l + B_l)\exp(i(\omega_l t + \varphi_l)) - (A_l - B_l)\exp(-i(\omega_l t + \varphi_l))]\exp(i\alpha_l). \tag{3.3}$$

A_l, B_l are the major and minor axis of the ellipses with orientation α_l and phase φ_l. These four real values of each tidal harmonic considered, as well as the mean current w_0, may be estimated by means of least-squares methods from a measured discrete time series w_n

$$\sum_n |w_n - w_0 - w_{Tn}|^2 = \epsilon^2 = \text{minimum}, \tag{3.4}$$

where n refers to the sampling time t_n. For computational convenience, complex amplitudes are introduced in (3.3)

$$w_l(t) = a_l \exp(i\omega_l t) + b_l \exp(-i\omega_l t), \tag{3.5}$$

with

$$a_l = \tfrac{1}{2} i(A_l + B_l)\exp(i(\alpha_l + \varphi_l)),$$
$$b_l = -\tfrac{1}{2} i(A_l - B_l)\exp(i(\alpha_l - \varphi_l)).$$

It should be mentioned that inserting (3.5) into (3.4) and solving the minimization problem leads to the same set of linear equations as applying the least-squares fit to the two components of the current vector separately (Godin, 1972).

By the approach (3.2) and (3.3), the different tidal harmonics are assumed to have constant amplitude and phase over the measuring time, i.e. the process is deterministic and the spectrum consists of a number of discrete lines. Due to the generating forces this should be the case, but because of interaction processes within the ocean, currents at tidal periods with time-dependent amplitude and phase may occur, representing a random contribution with broader spectra.

The optimal number L of tidal harmonics and the respective periods, to be inserted in (3.2) and (3.3), were determined by trial and error. The aim being to minimize ϵ^2, i.e. to explain by tides as much of the observed variance as possible. An increase in tidal variance leads to a decrease in ϵ^2 in (3.1). It appears that the semidiurnal tide M2 (12.42 h) dominates the tidal field and by considering the additional tidal harmonics S2 (12.0 h), N2 (12.7 h), K1 (23.9 h) and O1 (25.8 h), ϵ^2 may be reduced by about 10%. By adding other tidal harmonics, no further important decrease of ϵ^2 can be achieved. Thus, for removing tides, we only take into account the five harmonics mentioned.

Interference of tides with similar periods may lead to incorrect estimates of tidal parameters. This is illustrated in Fig. 5. The upper part displays the current velocities of the 1990 mooring at the deepest horizon at 427 m, see Fig. 3a. The variation in tidal amplitudes as visible in the time series is obviously due to the interference of the different semidiurnal tides. For three sections of equal length, tidal ellipses are presented in the lower part of Fig. 5 (solid lines). The stick represents the horizontal current vector at time $t = 0$. During one tidal period the vector rotates along the ellipse in the direction indicated by the arrow.

The time series are fitted by the M2 only (upper panel) and by a superposition of S2, M2, N2, K1 and O1 (lower panel). For reference, tidal ellipses as deduced from the total series are also determined and displayed (dashed lines). The axes of the tidal ellipses from the three sections show considerable differences, both in dependence on the section selected and on the number on tidal harmonics used. Regarding the whole time series the latter dependence vanishes. Thus, it may be concluded that a time series of some 800 h is necessary for reliably resolving the M2. This value matches well the reciprocal frequency difference of the M2 and N2 semidiurnal tides, $(\nu_{M2} - \nu_{N2})^{-1} \approx 600$ h.

Figure 6a shows the M2 tidal ellipses for all depths horizons available from the 1990 mooring. In accordance with Fig. 4 the lengths of the time series are 810 h, and fitted by the five tides mentioned. Fitting by only M2 yields nearly identical results. Horizontal current vectors, represented by sticks, are displayed every hour. The respective depths are indicated. The M2 tide is relatively stable as a function of depth. The decrease in speed between the 67 m and 59 m horizons is obviously due

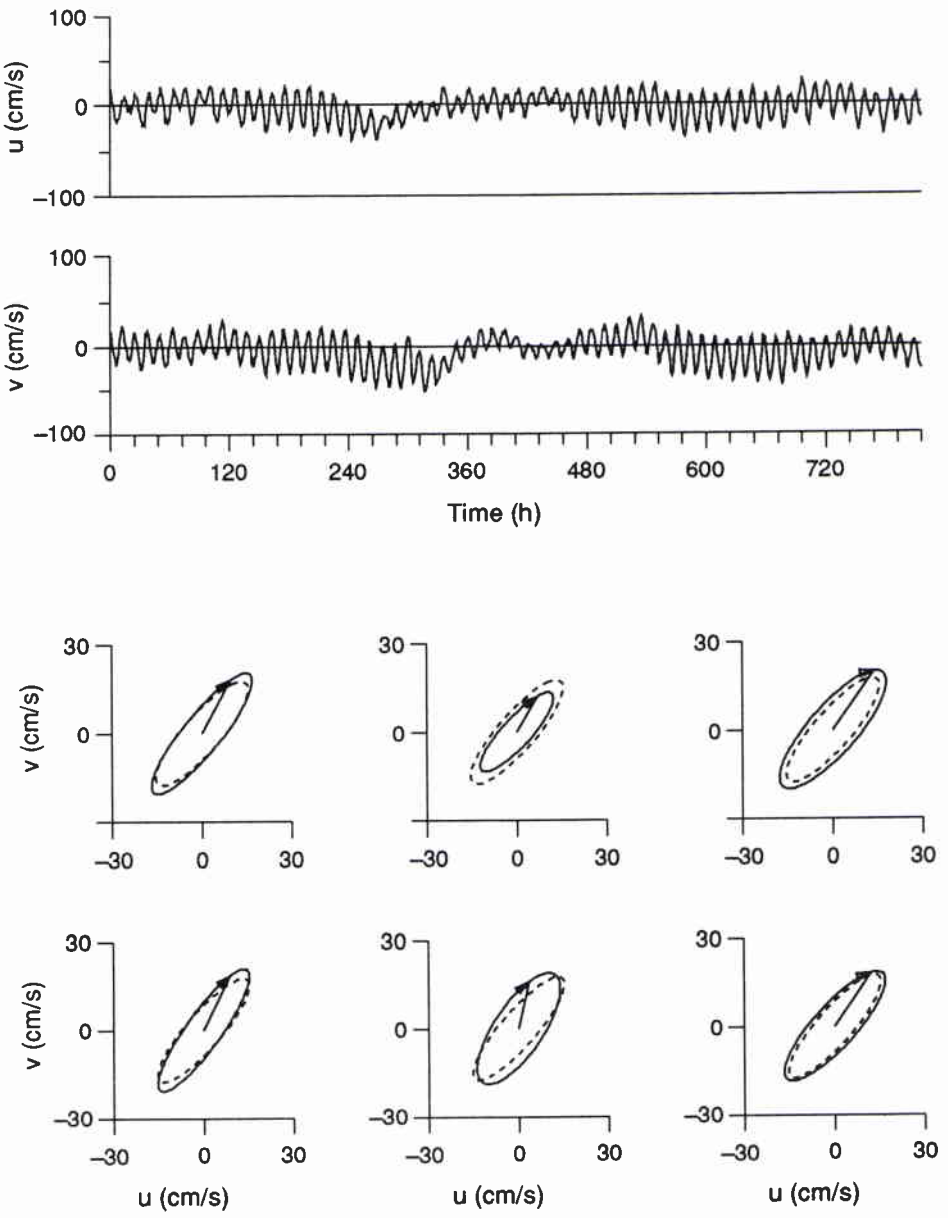

Figure 5 *Current velocities (1990 mooring, 427 m) and M2 ellipses. M2 ellipses are computed from 3 partial series of 270 h (solid line), and from the full series of 810 h (dashed line), with fitting by M2 only (upper panel) and S2, M2, N2, K1 and O1 (lower panel).*

to contamination by sidelobe reflections, as discussed earlier. The tidal ellipses are minimal at 59–51 m and then increase with decreasing depth, reaching the same size as in the deeper ocean at 35–27 m. As discussed earlier, there is some evidence from scattering geometry that contamination due to sidelobe reflections becomes less important on approaching the sea surface. Time series at the uppermost level of

19 m contain some spikes and the respective ellipse has to be regarded with caution.

Figures 6b and 6c show the vertical dependence of M2 tidal ellipses as observed at the beginning and end of the half-year moorings of 1991/92, which was carried out with a lower vertical resolution. The time series investigated correspond to those of Fig. 4 (middle and right panels). The lengths and the fitted tides are the same as in Fig. 6a. Figure. 6b shows a strong variation of the M2 tide with depth. The upper four horizons may be contaminated by sidelobe reflections but the 72 m and 88 m horizons also indicate a decrease of tidal currents at lower depths. This behaviour is even more obvious in the following three partial time series (not shown here), but is not present for the last two. Figure 6c displays the vertical dependence of the M2 tide for the last of 6 partial time series.

Table 2 summarizes some results of the tidal analysis. Vertically averaged current velocities are investigated, where the averaging extends over all horizons not contaminated by sidelobe reflections, i.e. below the dotted line in Fig. 4. The length of the time series are 810 h, one from the 1990 mooring and six from the 1991/92 mooring. Start times of the series are indicated. Major (A) and minor (B) axes and orientation (α) of the M2 ellipse are presented. Positive B indicates clockwise rotation. In addition, the ratio of variance of the M2, S2, N2, K1 and O1 tide with respect to the total variance are listed. The M2 tide contains some 60% of the total variance, while only the S2 tide contains more than 5% for all partial series.

Considering the 1991/92 mooring, the M2 is relatively stable over the 6 partial time series, both in amplitude and in orientation. Thus, these values may be interpreted as the barotropic tide. The somewhat smaller tidal amplitudes of the last two partial series may be explained by the different depth dependence of the M2 and the fact that the averaging only extends over about 75% of the water column. Indeed, by averaging over all horizons available, i.e. including those which may be contaminated by sidelobe reflections, the agreement of M2 parameters of the 6 partial series becomes even better, with the mean of both amplitudes A_{M2} and B_{M2} decreasing by about 1 cm/s and their variance by more than 50%. In spite of the questionable accuracy of near-surface data, it may be stated that the vertically averaging ADCP allows a more reliable determination of the barotropic tide than is possible from conventional current meters.

The same analysis as for Table 2 has been applied to near-surface currents (see Table 3. In order to avoid contamination from spikes and surface waves on the one hand, and contamination from sidelobe reflections on the other, the second uppermost horizon has been chosen, which is centred at 27 m for the 1990 mooring and at 24 m for the 1991/92 mooring.

The variance ratio of the M2 tide with respect to the total variance is considerably smaller for near-surface currents than for those of the deeper ocean. Reasons for this finding are the higher natural variance, but also contaminations due to sidelobe

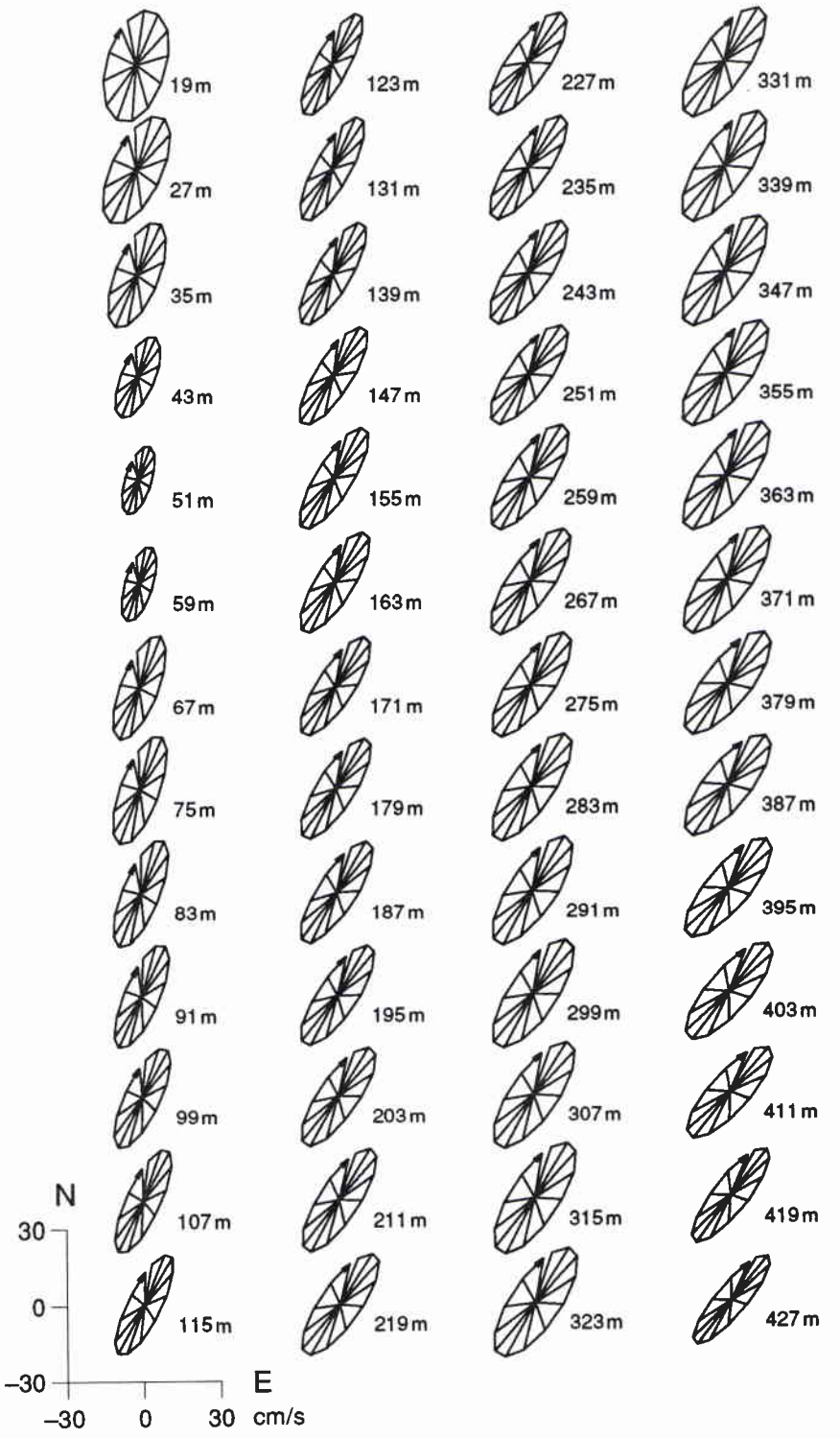

Figure 6a *M2 tidal ellipses as function of depth (1990 mooring), time series of 810 h fitted by S2, M2, N2, K1 and O1. Hourly current velocities are represented by sticks, with north component upwards, and east component to the right. The phase refers to Julian day 90/196.00.*

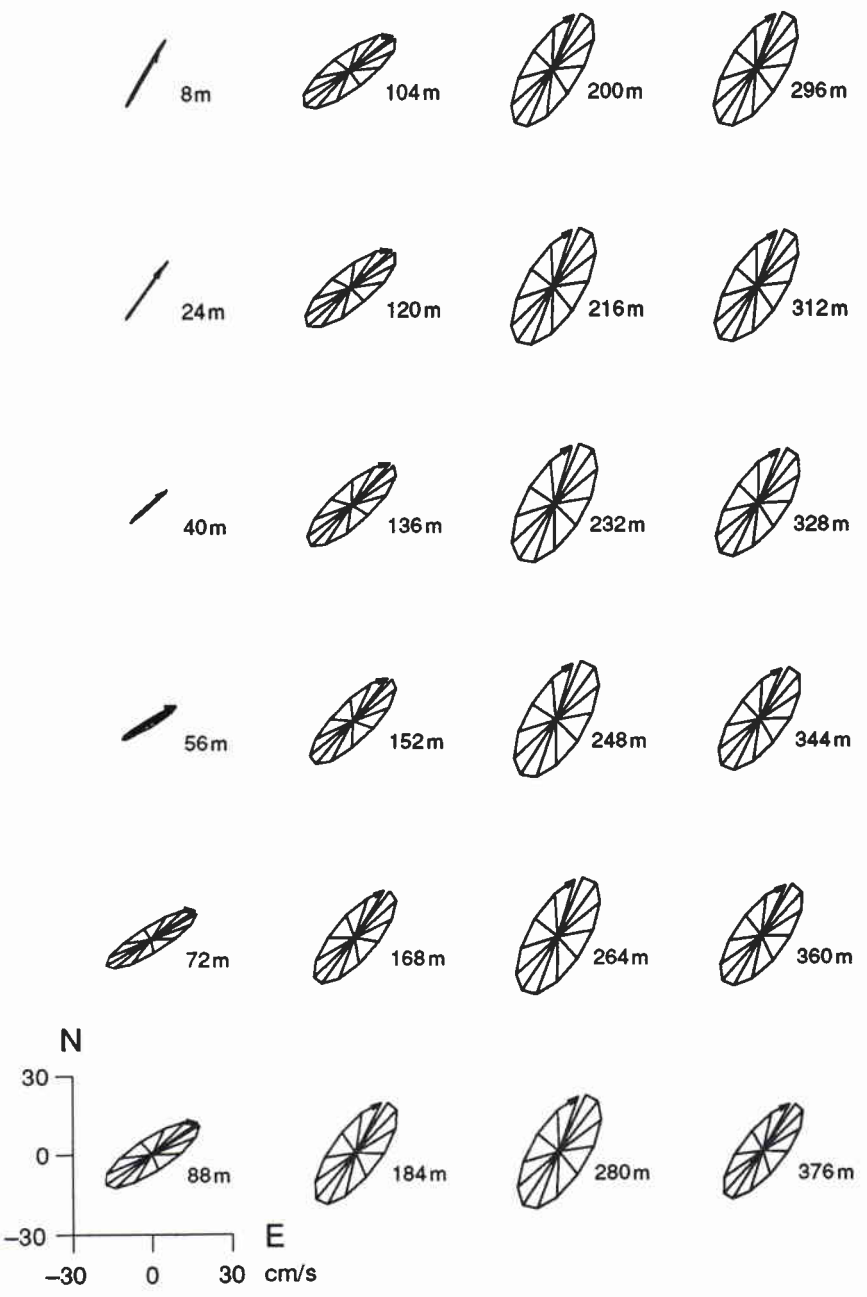

Figure 6b *M2 tidal ellipses as function of depth (1991/92 mooring), first partial 810 h time series, fitted by S2, M2, N2, K1 and O1. The phase refers to Julian day 91/229.00. For further explanation see Fig. 6a.*

reflections may be important. A surprisingly low ratio is found for the first 4 partial series of the 1991/92 mooring.

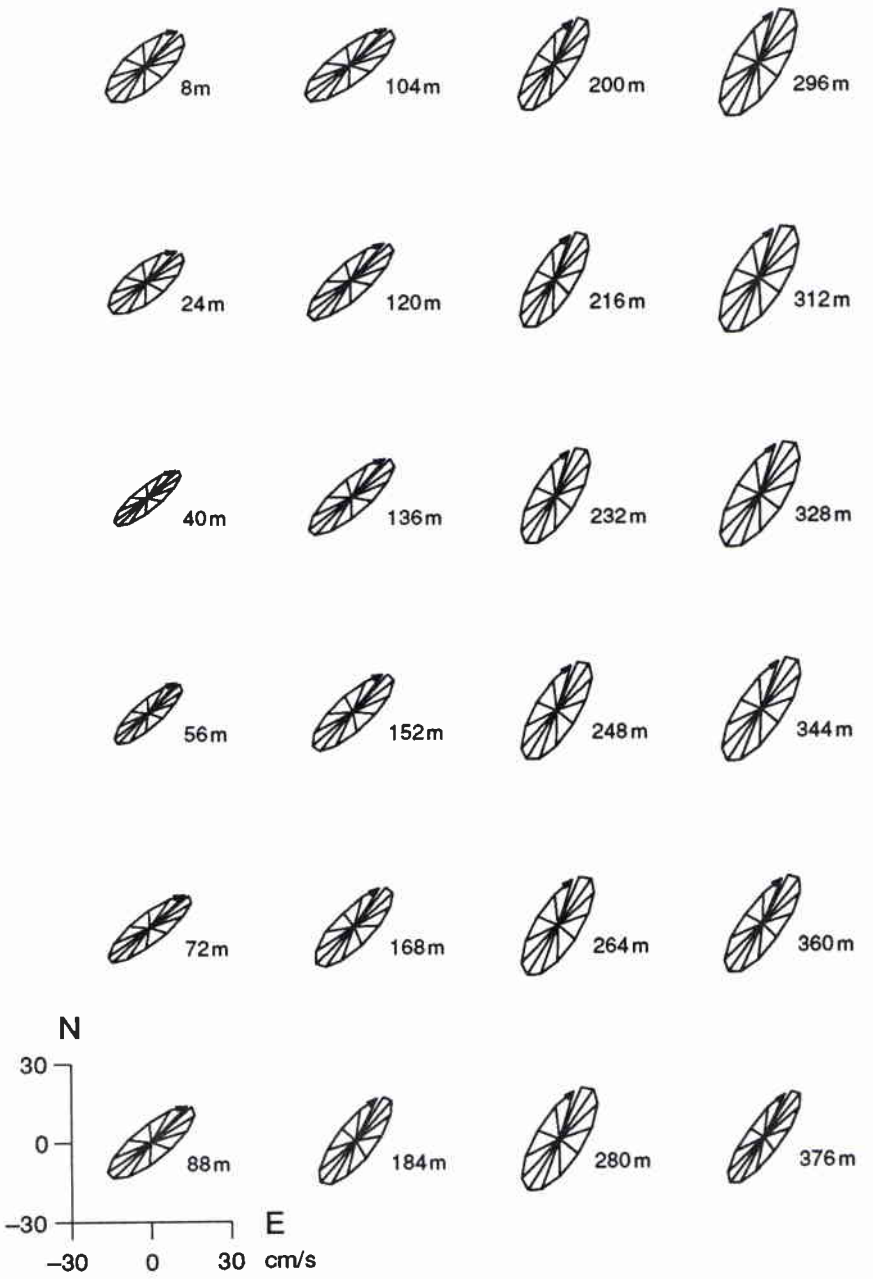

Figure 6c *M2 tidal ellipses as function of depth (1991/92 mooring), last partial 810 h time series, fitted by S2, M2, N2, K1 and O1. The phase refers to Julian day 92/32.75. For further explanation see Fig. 6a.*

Table 2 *M2 tidal ellipses and variances of M2, S2, N2, K1 and O1, of vertically averaged currents*[1]*, from 810 h time series*[2,3]

Time	A_{M2}	B_{M2}	α_{M2}	σ^2_{M2}	σ^2_{S2}	σ^2_{N2}	σ^2_{K1}	σ^2_{O1}
90/196.00	23.7	7.8	33.8	0.66	0.09	0.02	0.02	0.01
91/229.00	22.5	8.2	38.9	0.73	0.14	0.04	0.01	0.02
91/262.75	23.1	8.4	39.3	0.53	0.08	0.01	0.02	0.01
91/296.50	21.2	7.2	39.7	0.62	0.08	0.02	0.03	0.03
91/330.25	22.0	8.5	39.6	0.65	0.05	0.04	0.04	0.04
91/364.00	20.4	6.7	39.2	0.62	0.07	0.04	0.05	0.04
92/32.75	21.4	7.2	38.7	0.57	0.11	0.03	0.02	0.02

[1] Below dashed line in Fig. 4.
[2] Starting at the Julian day indicated.
[3] A[cm/s] = major axis, B[cm/s] = minor axis, α[deg] = orientation and σ^2 = ratio of variance of indicated tidal component to total variance.

Table 3 *M2 tidal ellipses and variances of M2, S2, N2, K1 and O1 of near-surface currents*[1,2]

Time	A_{M2}	B_{M2}	α_{M2}	σ^2_{M2}	σ^2_{S2}	σ^2_{N2}	σ^2_{K1}	σ^2_{O1}
90/196.00	23.1	9.9	25.2	0.19	0.04	0.00	0.01	0.00
91/229.00	13.5	0.1	36.4	0.05	0.01	0.03	0.01	0.01
91/262.75	12.4	0.0	39.3	0.05	0.02	0.00	0.02	0.00
91/296.50	14.6	1.4	38.1	0.07	0.01	0.00	0.00	0.01
91/330.25	13.1	1.4	47.4	0.07	0.02	0.01	0.01	0.01
91/364.00	16.9	5.6	42.7	0.15	0.03	0.01	0.01	0.01
92/32.75	17.3	7.0	52.5	0.14	0.07	0.01	0.01	0.02

[1] Second uppermost horizon in Fig. 4.
[2] For further explanation see Table 2.

4

Frequency spectra

Frequency analysis of two-dimensional current vectors may be carried out for both components separately in Cartesian coordinates. Another possibility is to decompose the vector time series into clockwise and anticlockwise rotating portions. This method yields more physical information, and has been applied for our analysis. Physical processes to be investigated are assumed to be random, including inertial motions. These motions occur as wave groups of limited duration with random phases. The corresponding spectrum extends over a finite frequency range, in contrast to line spectra of deterministic tides.

For computing rotational spectra, it is convenient to represent the two-dimensional current vector by a complex number, cf. (3.1). Variance spectra presented are computed via the finite discrete fourier transform,

$$c_k = \frac{1}{N} \sum_{n=0}^{N-1} w_n \exp(\frac{2\pi i k n}{N}), \qquad k = -\tfrac{1}{2}N + 1, \ldots, \tfrac{1}{2}N. \tag{4.1}$$

The negative values of k refer to negative frequencies describing vectors rotating anticlockwise, while positive k refer to positive frequencies and clockwise rotation. The rotational variance spectra are defined by

$$\begin{aligned} S_{Ak} &= \langle c_k c_k^* \rangle, \qquad k = -1, \ldots, -\tfrac{1}{2}N + 1, \\ S_{Ck} &= \langle c_k c_k^* \rangle, \qquad k = \ \ 1, \ldots, \ \ \tfrac{1}{2}N - 1, \end{aligned} \tag{4.2}$$

where the indices A and C refer to anticlockwise and clockwise rotation, respectively. The angled brackets indicate spectral averaging, as may be performed in different ways and will be discussed later. Frequency scales are determined by the length of the time series and the sampling rate. The variance spectra are normalized to represent the total variance of the time series. Mean currents ($k = 0$) are not considered in this analysis.

For analysing random time series, a compromise has to be found between the required frequency resolution and statistical confidence. The inertial frequency at the latitude of the two moorings (about 64°50′N) is

$$f = 13.24 \text{ h}, \tag{4.3}$$

which is quite close to the dominating semidiurnal tide M2 of 12.42 h. The difference in these periods corresponds to the frequency resolution of a time series of 210 h

duration. In addition, the tidal analysis shows some evidence for variance being present at N2 with a 12.7 h period, making the detection of inertial motions even more complicated.

For obtaining reasonable statistical confidence, some averaging in frequency space has to be performed, which reduces the spectral resolution. The time series as investigated in the previous sections are of 810 h duration and taken at different depths. For analysing currents at a single depth horizon, the respective time series are segmented into 9 parts with 50% overlap and multiplied by a Hanning window. The partial time series are of 162 h length and about 13 times the period of the dominating M2 tide. The variance spectra are obtained by adding up the spectra of the partial time series. These procedures are equivalent to a certain weighted average in frequency space, yielding about 16 degrees of freedom (Nuttall, 1971). The corresponding confidence limits are taken from Jenkins and Watts (1969) and are in good agreement with the spectral variability as obtained from normal-distributed white noise, averaged as described. The half-year mooring of 1991/92 allows for a higher statistical confidence by considering more than one successive 810 h time series.

Figures 7a and 7b display rotational variance spectra of the 1990 mooring at the lowest level of 427 m and the second uppermost level of 27 m. Two options are investigated, time series containing tides (upper panels) and those from which the tides S2, M2, N2, K1 and O1 have been removed. As result of the discussion in Sect. 3, the removal is applied to time series of 810 h length which is about the total length for this mooring. The vertical dashed lines indicate the periods of 24 h, the inertial motion f and the semidiurnal tide M2 (from left to right). Spectra containing tides (i.e. upper panels) show the dominant contribution of M2. Tidal ellipses, as shown in Sect. 3 can be represented by two vectors of different amplitudes rotating in opposite directions and causing contributions to both spectra S_{Ak} and S_{Ck}. Clockwise rotating currents contain higher variance at the diurnal period as compared to anticlockwise rotating currents.

Considering the 427 m horizon (Fig. 7a), tidal removal eliminates all semidiurnal variance remaining for anticlockwise rotating currents, but there is considerable variance left for clockwise rotating currents. This behaviour indicates the presence of inertial motions, but is also consistent with contributions from semidiurnal internal tides, which, due to the small difference in semidiurnal and inertial period, rotate nearly circularly in the area considered. The broad spectrum around the inertial frequency may be explained by relatively short events of inertial oscillation. Another finding is that the high-frequency tail of the spectrum is about white in the case of anticlockwise rotating currents but shows an approximate $\nu^{-1.6}$-decay for clockwise rotating currents. The spectra from the 27 m horizon (Fig. 7b) contain considerably more variance at all frequencies, except tidal, than those in the deeper ocean.

Figures 8a and 8b display spectra from the 1991/92 mooring. In order to obtain higher statistical confidence, spectra of three successive 810 h time series are added, covering the period from Julian day 91/229 to 91/330. These spectra are again from

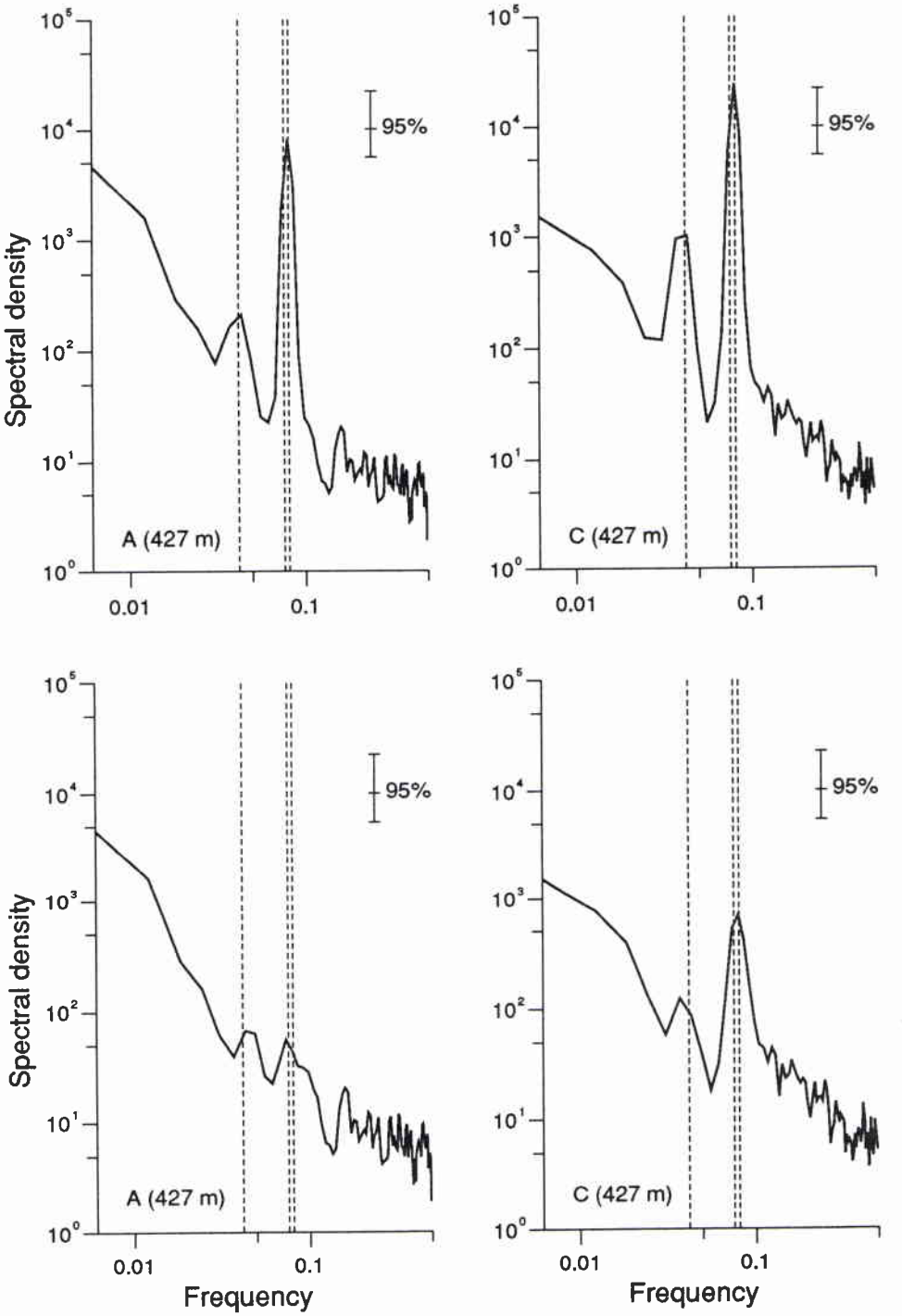

Figure 7a *Rotational variance spectra (1990 mooring, 427 m), of anticlockwise (A) and clockwise rotating (C) currents. Dimension of frequency is* $[h^{-1}]$ *and of spectral density* $[(ms^{-1})^2\ h]$. *The upper panel refers to 810 h time series containing tides, the lower to time series with tides S2, M2, N2, K1 and O1 removed. Dashed vertical lines represent 24 h, inertial, and M2 periods.*

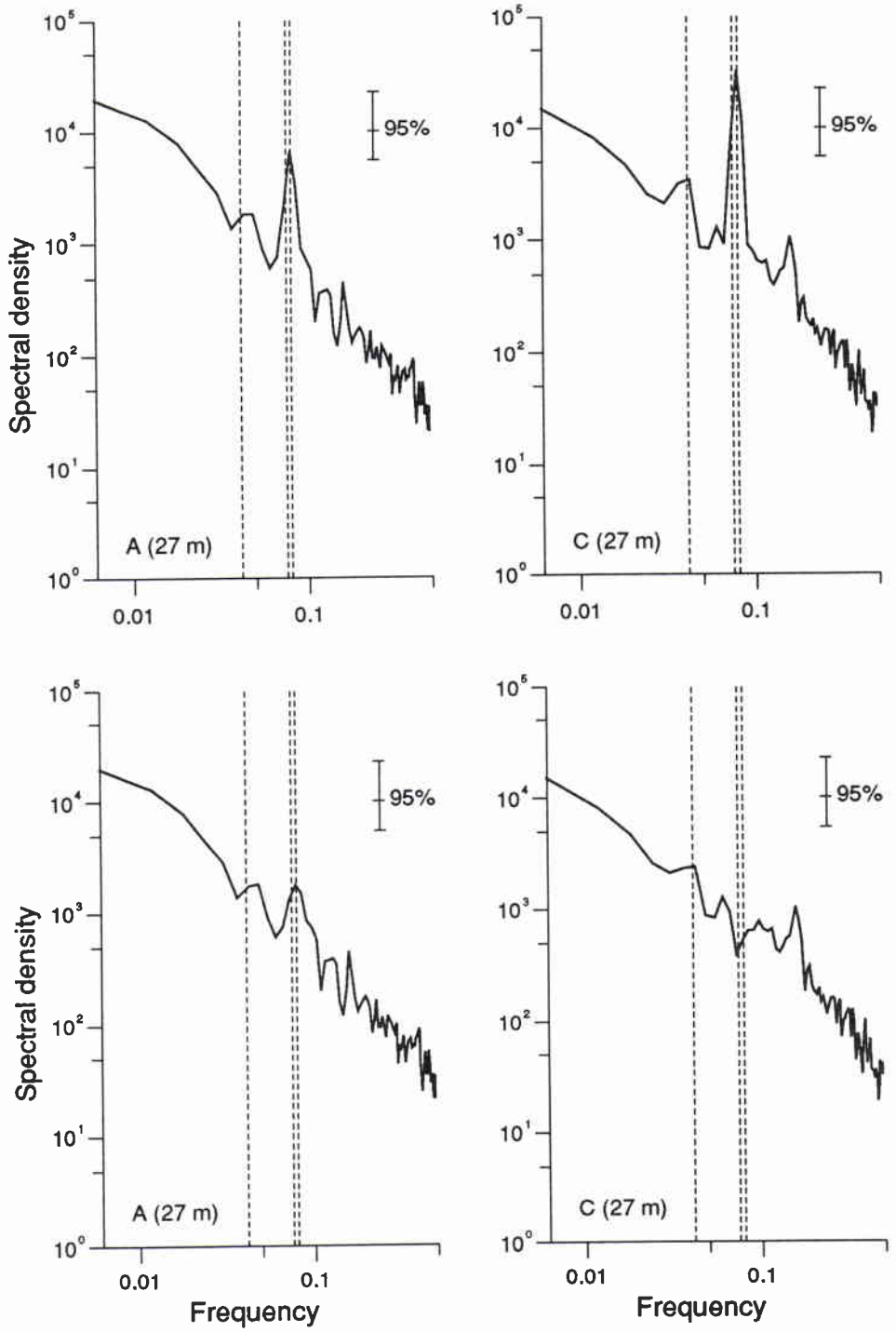

Figure 7b *Rotational variance spectra (1990 mooring, 27 m). For further explanation see Fig. 7a.*

the deepest 376 m horizon (Fig. 8a) and the second uppermost at 24 m (Fig. 8b). Figures 9a and 9b contain average spectra of the period from Julian day 91/330 to 92/66. The general features, as discussed for the 1990 spectra (Figs. 7a,7b) are the same also for both parts of the longer-term 1991/92 mooring. Also the high-frequency tail of anticlockwise rotating currents is nearly white, while it decays by about ν^{-2} for clockwise rotating currents, i.e. somewhat stronger than for the 1990 mooring.

Near-surface currents as represented by the spectra of Figs. 7–9 show different frequency dependencies at the high frequency tail for anticlockwise ($\sim \nu^{-1.6}$) and clockwise rotating currents ($\sim \nu^{-2.2}$). About the same behaviour is found for all mooring periods investigated.

For considerably increasing the spectral resolution, fourier transforms have to be taken from longer partial time series, e.g. from the 810 h series. The loss of statistical confidence may partly be compensated by averaging spectra from different depths. As for the determination of the barotropic tide, all depth horizons are used, which are not contaminated by sidelobe reflections, i.e. are below the dashed line in Fig. 4. Again, the time series are weighted by a Hanning window. As currents at different depths are not statistically independent (Sect. 5), the estimation of confidence limits becomes difficult and is not attempted.

Figure 10a–10c display vertically averaged variance spectra with a stretched section of the frequency axis. The spectra refer to the 1990 (810 h) and the first and second part of the 1991/92 mooring (3×810 h, each). Again, all spectra show very similar features. After tide removal, significant variance remains in a broad frequency band around the inertial frequency only for clockwise rotating currents. This energy may be due to inertial motions but also to semidiurnal internal tides. A separation of both processes is not possible.

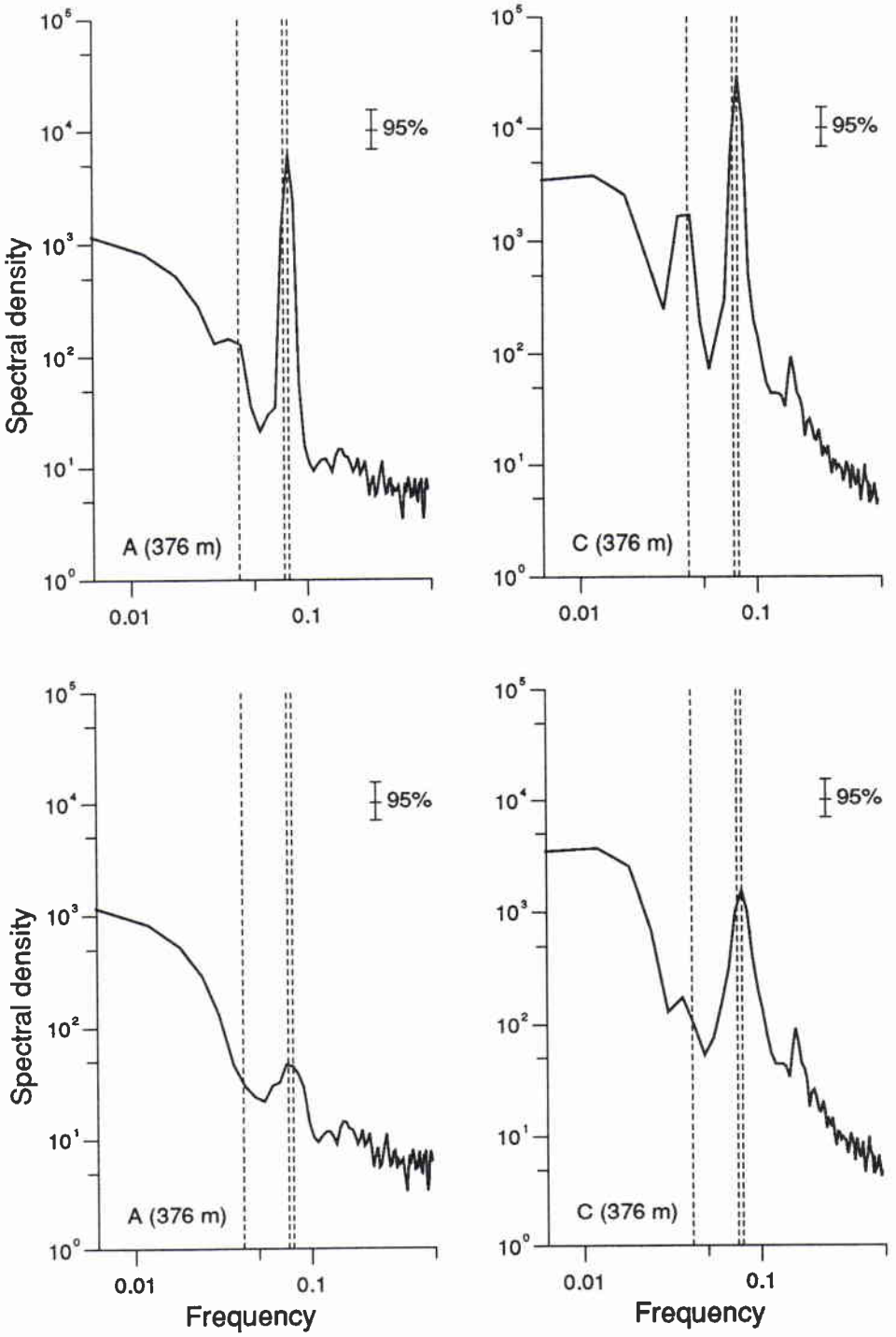

Figure 8a *Rotational variance spectra (1991/92 mooring, 376 m), average spectra of the first 3 partial 810 h time series. For further explanation see Fig. 7a.*

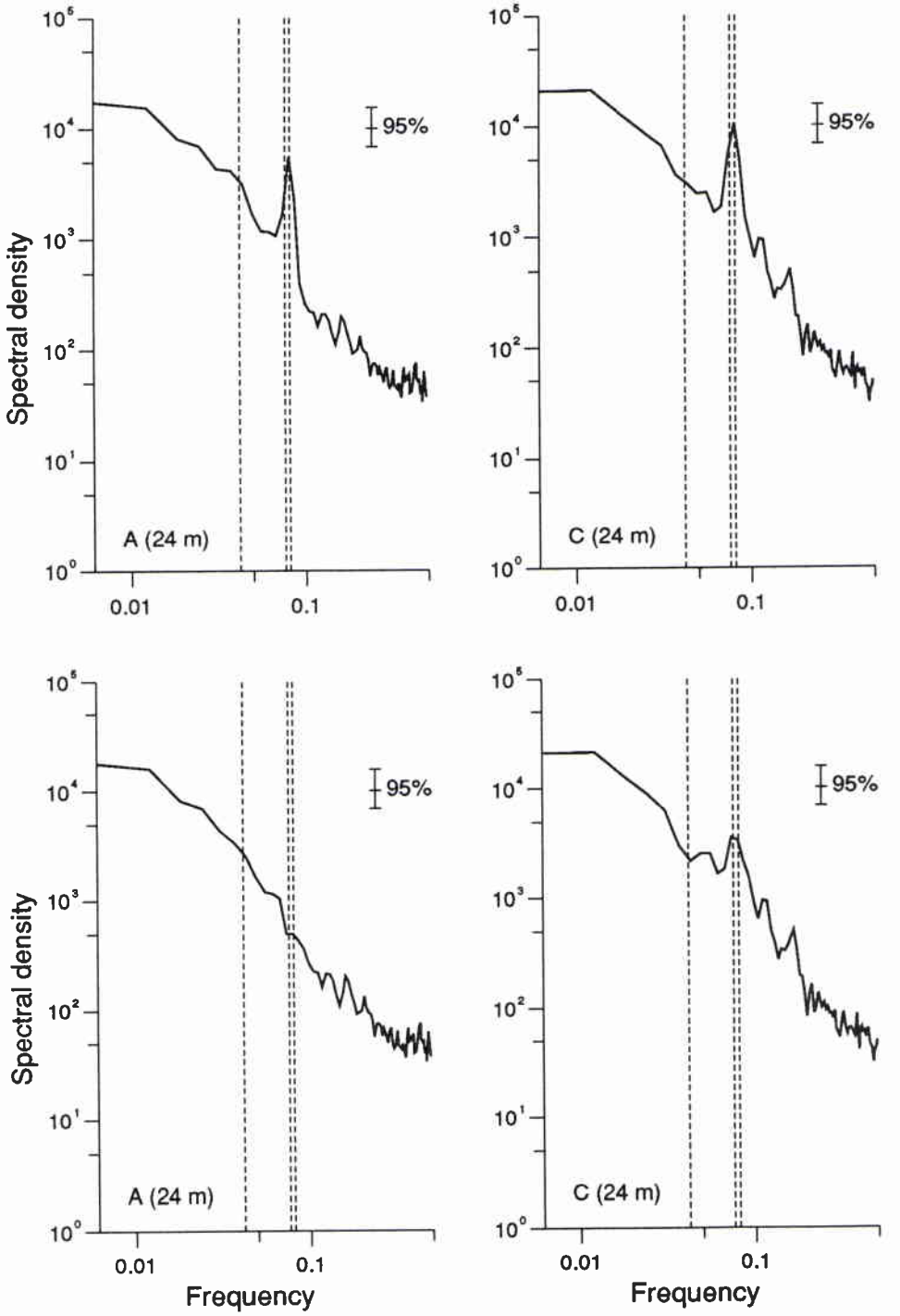

Figure 8b *Rotational variance spectra (1991/92 mooring, 24 m), average spectra of the first 3 partial 810 h time series. For further explanation see Fig. 7a.*

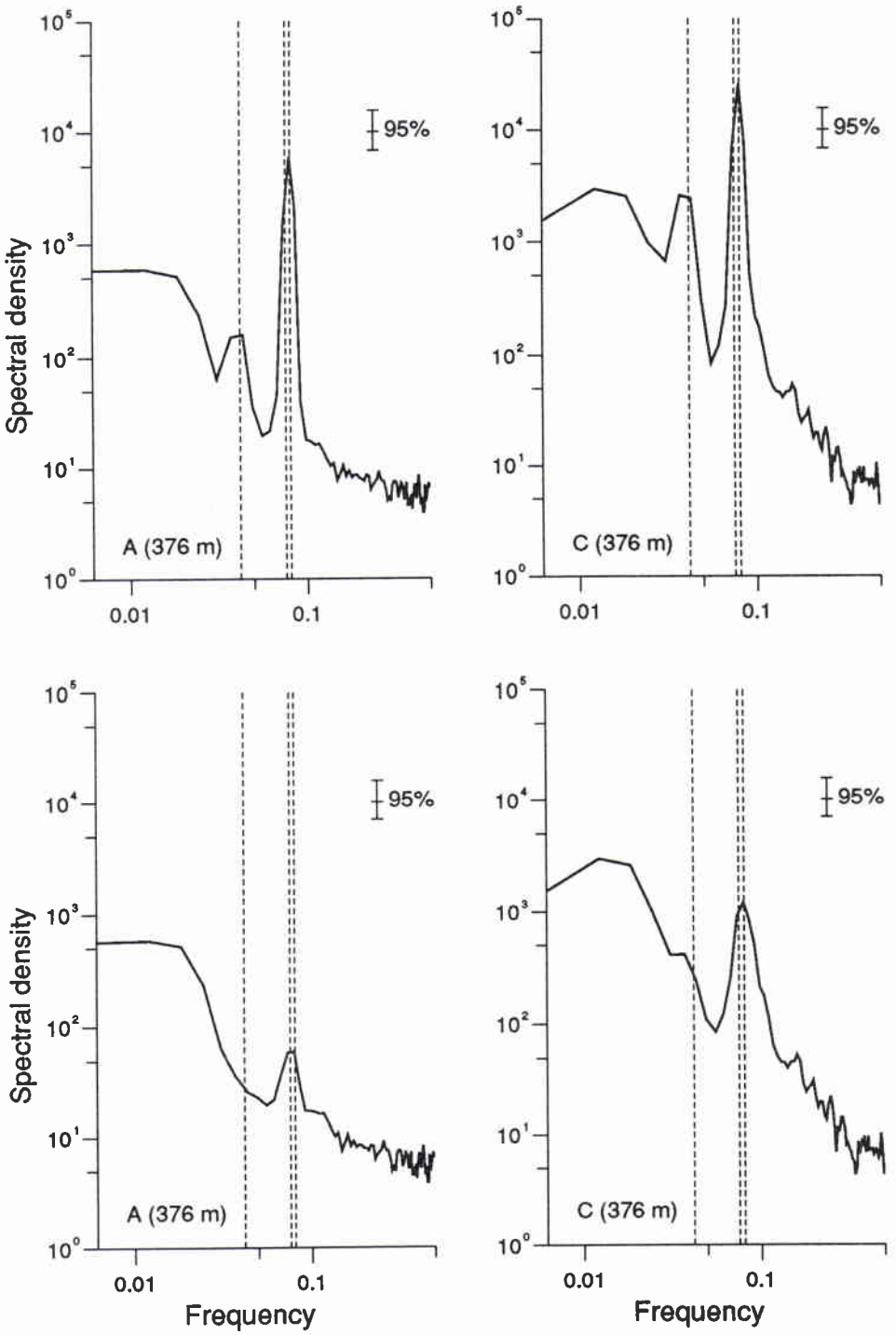

Figure 9a *Rotational variance spectra (1991/92 mooring, 376 m), average spectra of the last 3 partial 810 h time series. For further explanation see Fig. 7a.*

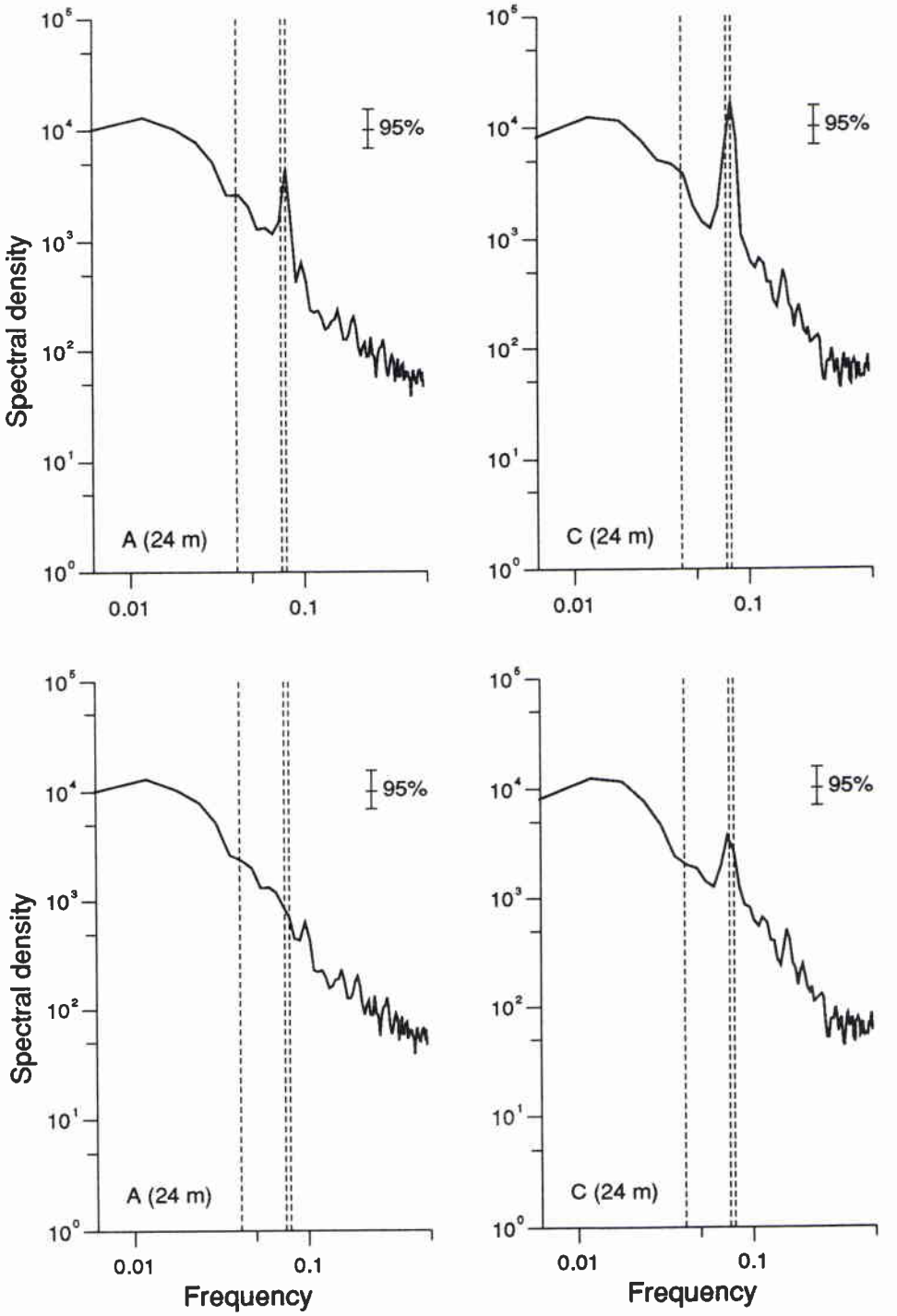

Figure 9b *Rotational variance spectra (1991/92 mooring, 24 m), average spectra of the last 3 partial 810 h time series. For further explanation see Fig. 7a.*

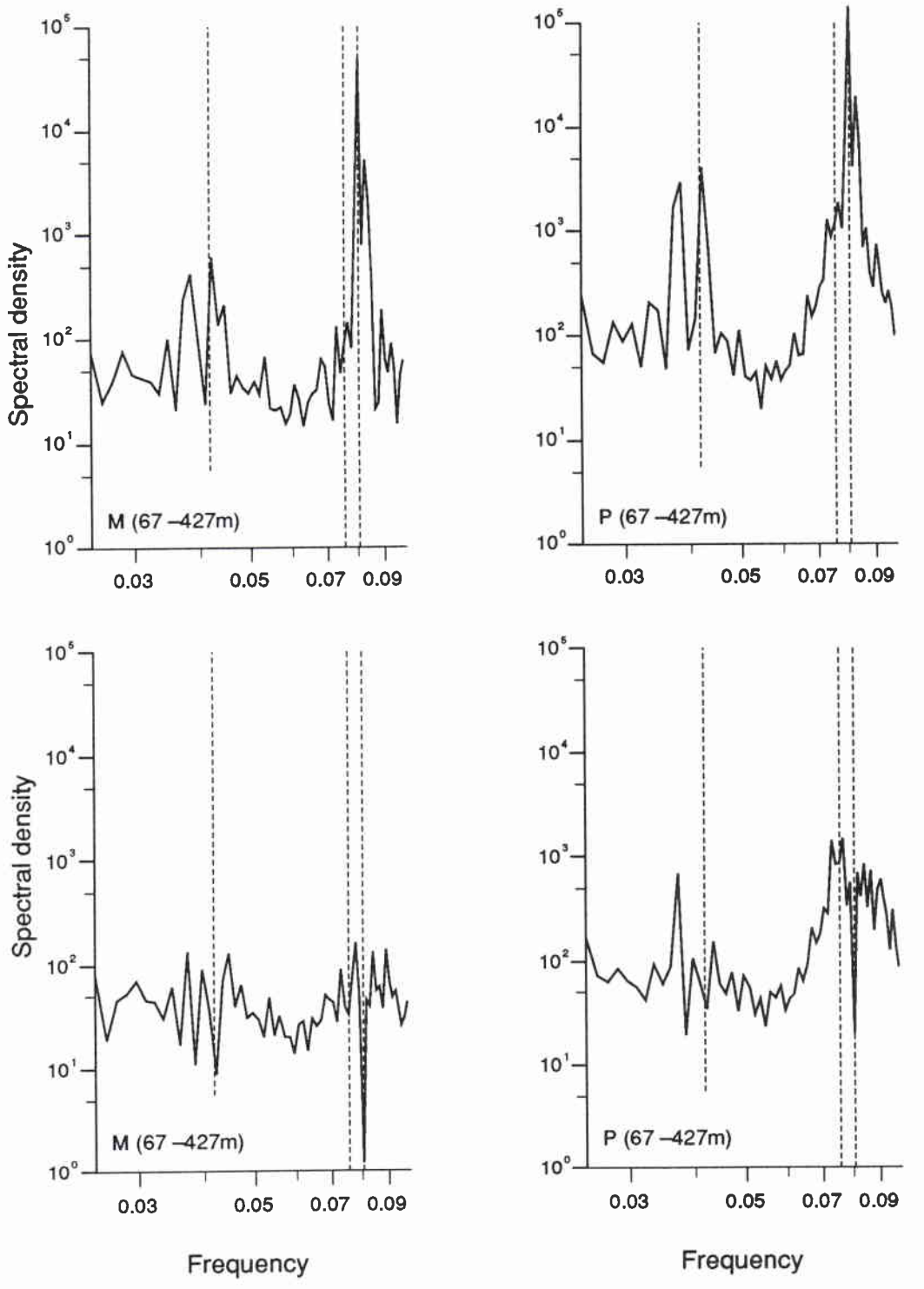

Figure 10a *Vertically averaged rotational spectra (1990 mooring), over depth horizons not contaminated by sidelobe reflections, from 810 h time series with full frequency resolution, (5× higher than in Figs. 7–9), only a section displayed. For further explanation see Fig. 7a.*

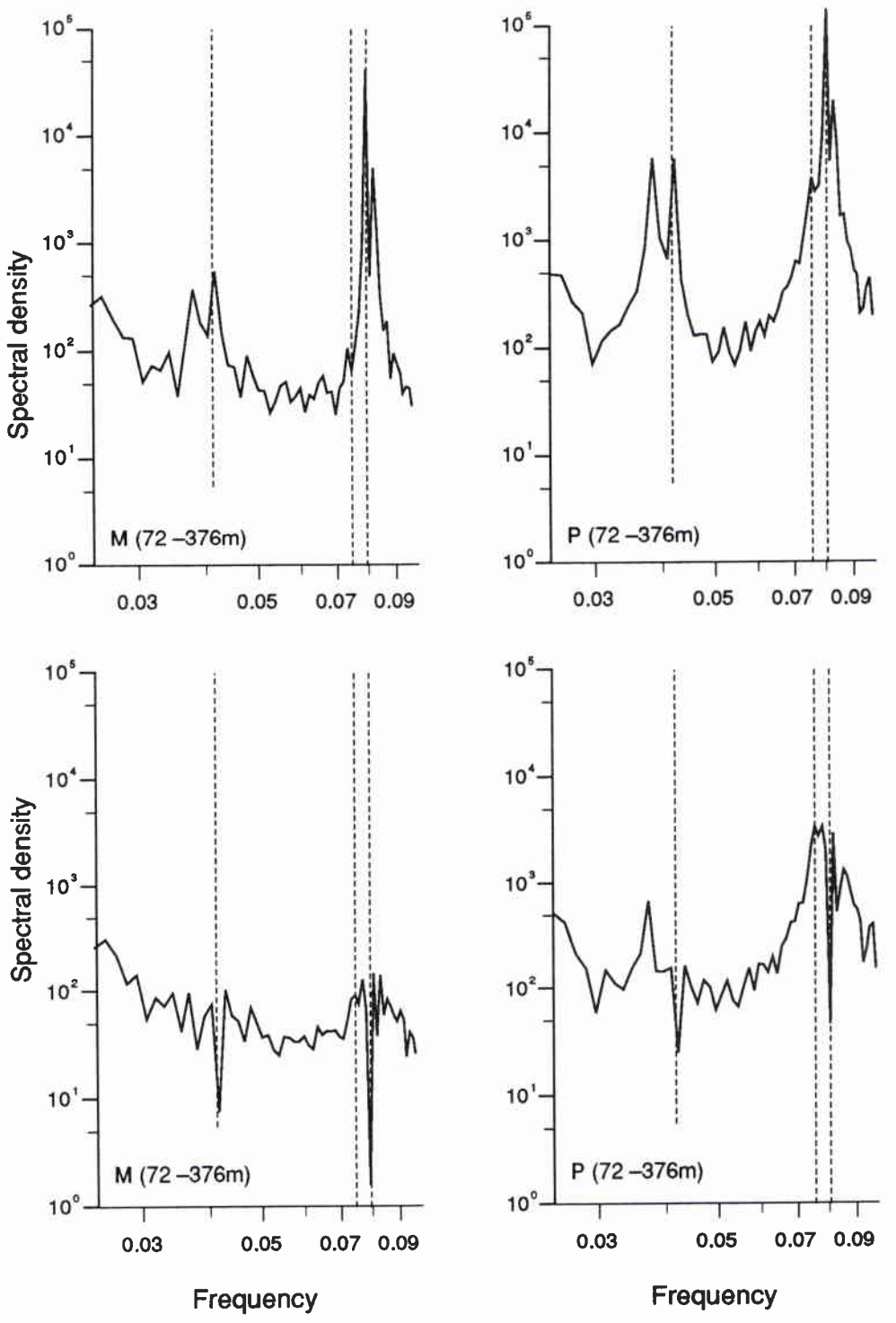

Figure 10b *Vertically averaged rotational spectra (1991/92 mooring), over depth horizons not contimated by sidelobe reflections, average spectra of the first 3 partial 810 h time series. For further explanation see Fig. 10a.*

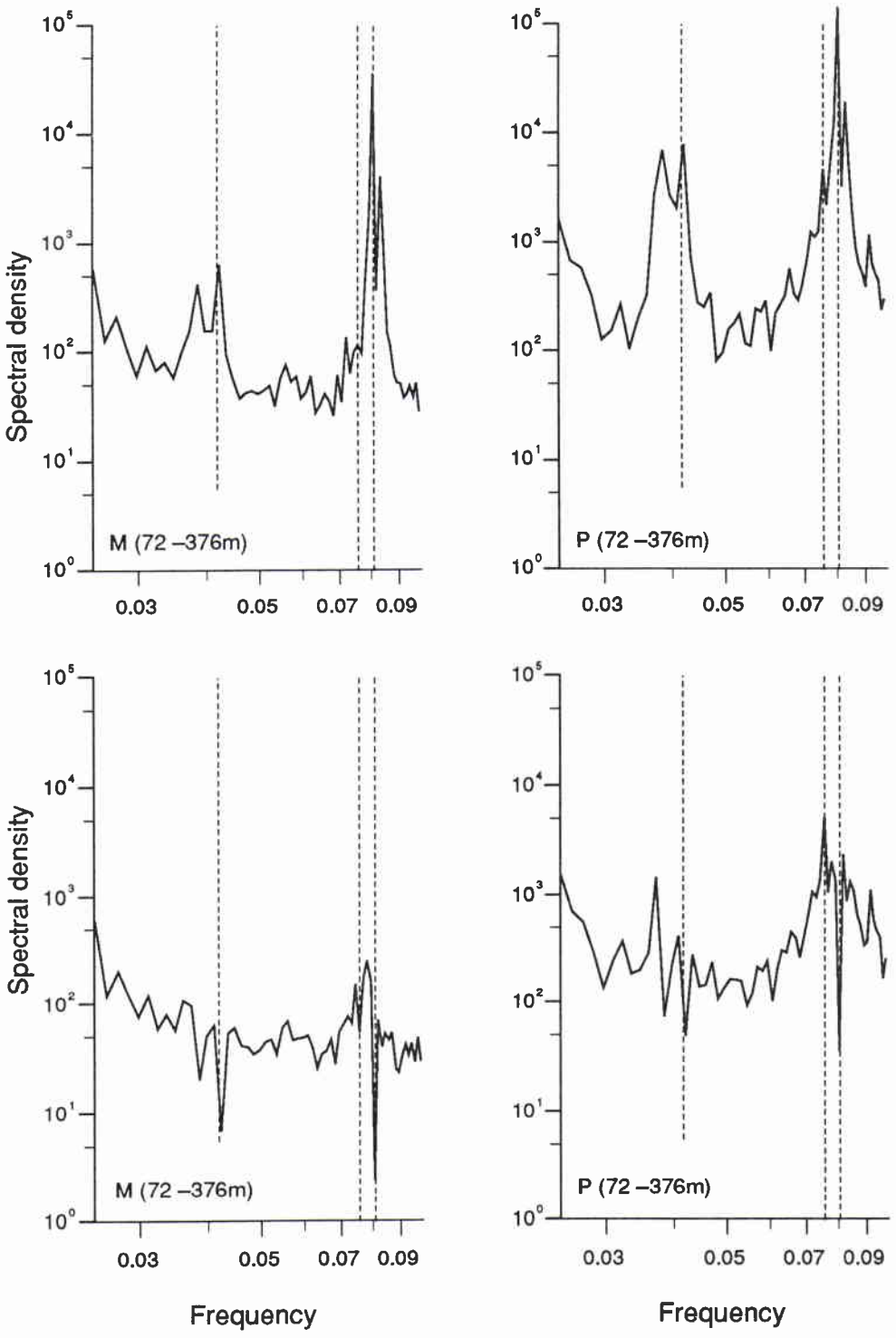

Figure 10c *Vertically averaged rotational spectra (1991/92 mooring), over depth horizons not contimated by sidelobe reflections, average spectra of the last 3 partial 810 h time series. For further explanation see Fig. 10a.*

5

Vertical coherence

Considering two complex time series w_a and w_b, measured at different depths, the complex coherence spectrum is defined by

$$K_k = \frac{\langle c_{ak} c^*_{bk} \rangle}{\sqrt{\langle c_{ak} c^*_{ak} \rangle \langle c_{bk} c^*_{bk} \rangle}}, \tag{5.1}$$

where c_{ak} and c_{bk} are the fourier coefficients of the two time series as defined by (4.1). As for the variance spectra, the coherence spectrum is divided into two parts representing currents rotating anticlockwise (A) and clockwise (C):

$$\begin{aligned} K_{Ak} &= \mid K_{Ak} \mid \exp(i\Phi_{Ak}), \quad k = -1, \ldots, -\tfrac{1}{2}N + 1, \\ K_{Ck} &= \mid K_{Ck} \mid \exp(i\Phi_{Ck}), \quad k = 1, \ldots, \tfrac{1}{2}N - 1. \end{aligned} \tag{5.2}$$

Both spectra are complex and are usually represented by their magnitude and phase. By definition, the magnitude is ≤ 1. We are mainly interested in the magnitude of coherence, which describes the linear dependence of the single fourier components. Again, the angled brackets in (5.1) denote spectral averaging. As the results are very similar from the different mooring periods, we only present coherence spectra from the first part of the 1991/92 mooring. Time series of 810 h length are analysed and used to remove tides. The coherence spectra are computed from 9 overlapping partial time series of 162 h duration, weighted by a Hanning window. Finally, the spectra of three successive 810 h series are averaged; the processing is analogous to that used for the variance spectra of Figs. 8a and 8b.

Instead of presenting confidence limits for the magnitude of the coherence spectrum, their significance is tested against the null hypothesis. Following Carter *et al.* (1973), 95% of estimated magnitudes of coherence will be less than about 0.45 in the case of real coherence being zero and estimated from 15 non-overlapping, Hanning weighted parts of the time series (5 from each 810 h series). Overlap as used may result in some approvement. Indeed, tests with random white noise show that 0.4 is a reasonable 95%-limit of zero coherence.

Figures 11a and 11b display the magnitude (solid line with dots) and phase (dashed line) of the coherence spectrum for anticlockwise and clockwise rotating currents. Current velocities are taken from adjacent depth horizons, close to the bottom (Fig. 11a) and to the surface (Fig. 11b). The upper panels refer to currents containing tides, the lower panels to currents with the tides S2, M2, N2, K1 and O1

removed. Periods of 24 h, inertial motion, and M2 tide are marked on the frequency axis.

Figure 11a shows nearly perfect coherence at periods longer than diurnal and around the semidiurnal period (upper panel). In between a significant decrease of coherence is visible. For semidiurnal periods, removing the tides does mainly affect anticlockwise currents, while coherence remains high for clockwise rotating currents (lower panel). Again this is an indication of inertial motions or internal tides being of influence. Anticlockwise rotating currents show lower coherence at the short-frequency tail of the spectrum as compared to clockwise rotating currents. This is in agreement with the approximate white-noise tail of the respective variance spectra (Fig. 8a), indicating that no short-period currents are present and the respective variance is due to noise.

In Fig. 11b the same data processing is applied to adjacent near-surface horizons. The results are very similar to those of Fig. 11a, with even higher coherence at the high-frequency tail of the spectra. The overall high coherence is surprising as currents at the 8 m level contain orbital motions of surface waves and current measurements at both horizons may be contaminated by sidelobe reflections. The coherence of currents from adjacent depth horizons is similar to those of Figs. 11a and 11b over all the water column, except for cases containing the 40 m or 56 m depth horizons, which show considerably less coherence. Obviously, this is due to contamination by sidelobe reflections, which becomes less important nearer the surface, i.e. at the horizons investigated in Fig. 11b.

Figure 12a displays the coherence of currents at the deepest horizon (376 m) recorded and the uppermost not contaminated by sidelobe reflections (72 m). Very high coherence only occurs for the anticlockwise rotating semidiurnal tide, which is totally suppressed after tides have been removed. For clockwise rotating currents the semidiurnal coherence is considerably less and cannot be suppressed by removing tides. This may be explained by the interference of inertial motions. Except for very low frequencies, there is no significant coherence for anticlockwise currents and very little for clockwise rotating currents. Figure 12b, displaying the coherence of current at 72 m and 24 m depths, shows significant coherence only for semidiurnal periods.

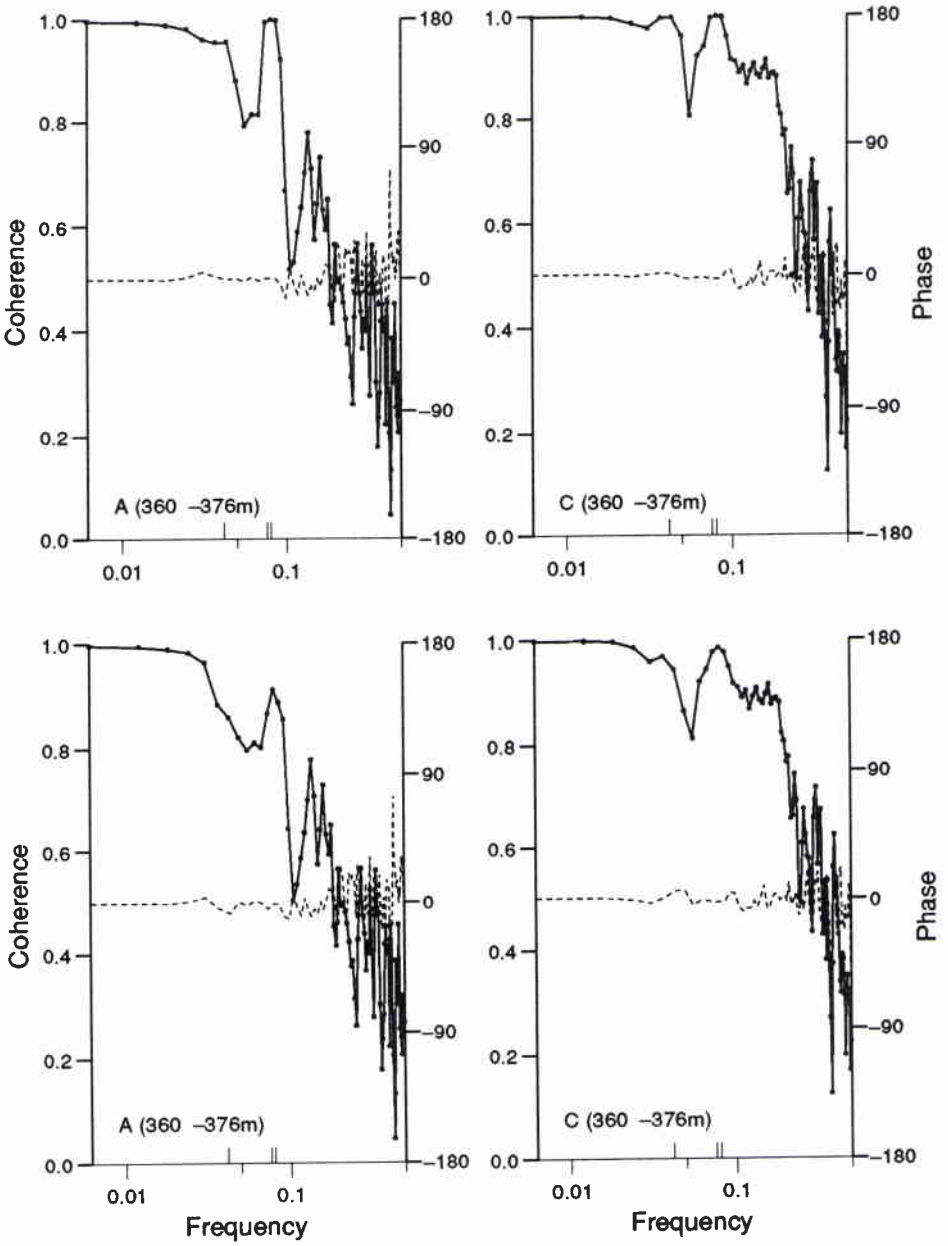

Figure 11a *Rotational coherence spectra (mooring 1991/92), from currents at adjacent bottom-close horizons: 360 m vs 376 m. Spectra are averages over the first 3 partial 810 h time series, representing anticlockwise (A) and clockwise rotating (C) currents. Solid lines display the magnitude of coherence, dashed lines the phase. The upper panel refers to 810 h time series containing tides, the lower to time series with tides S2, M2, N2, K1 and O1 removed. Marks on the frequency axis represent 24 h, inertial, and M2 periods.*

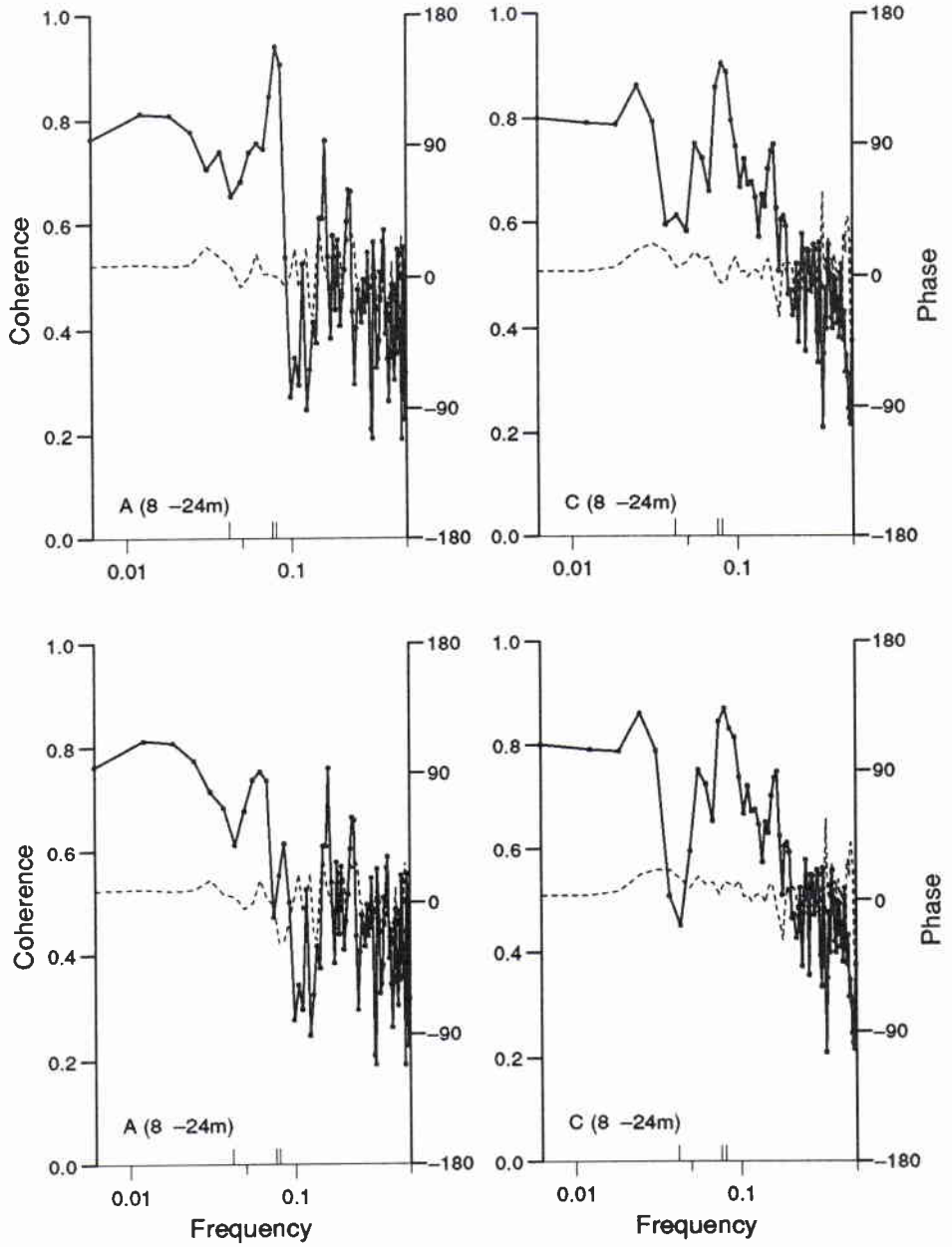

Figure 11b *Rotational coherence spectra (mooring 1991/92), from currents at adjacent surface-close horizons: 8 m vs 24 m. For further explanation see Fig. 11a.*

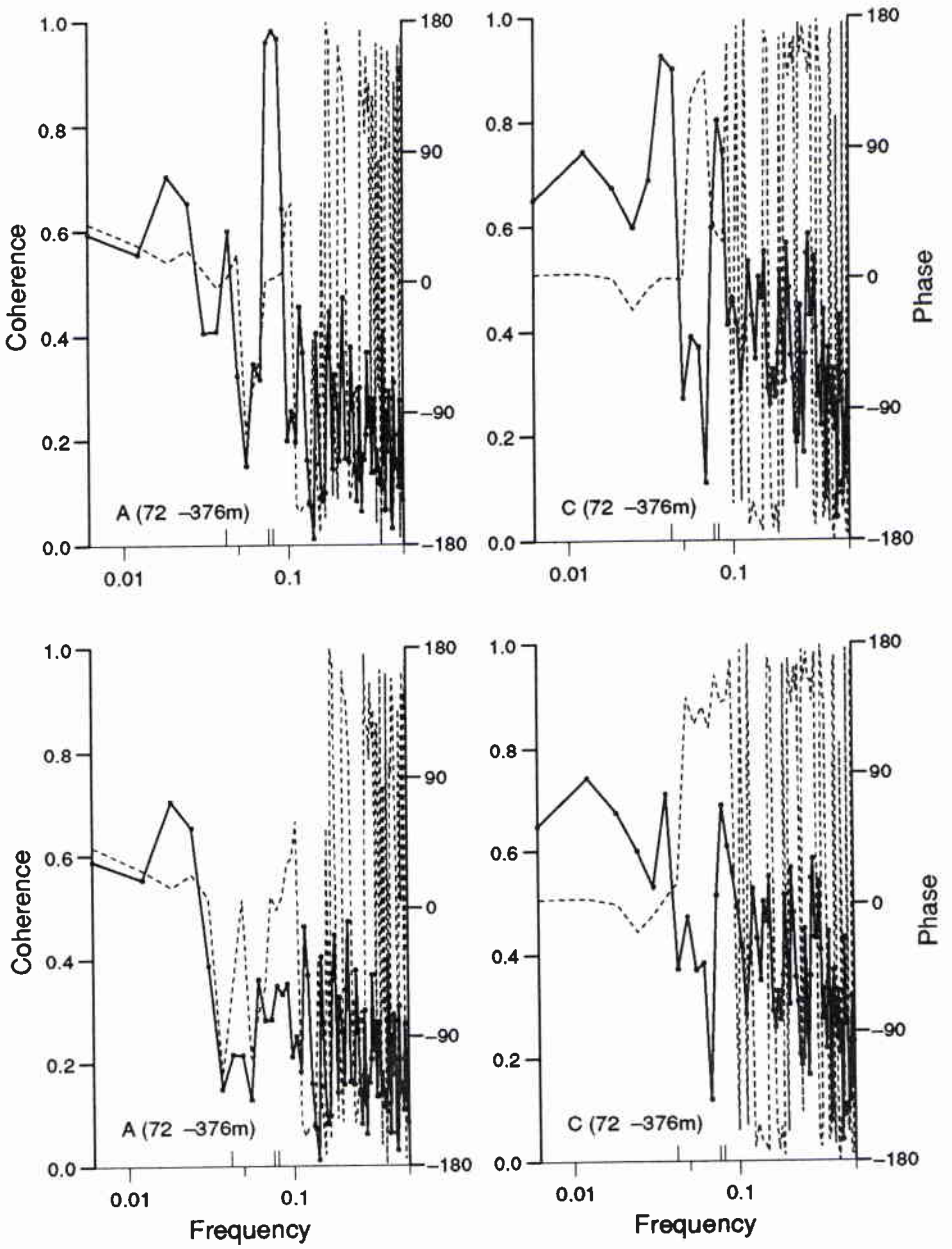

Figure 12a *Rotational coherence spectra (mooring 1991/92), from currents at distant horizons: 72 m vs 376 m. For further explanation see Fig. 11a.*

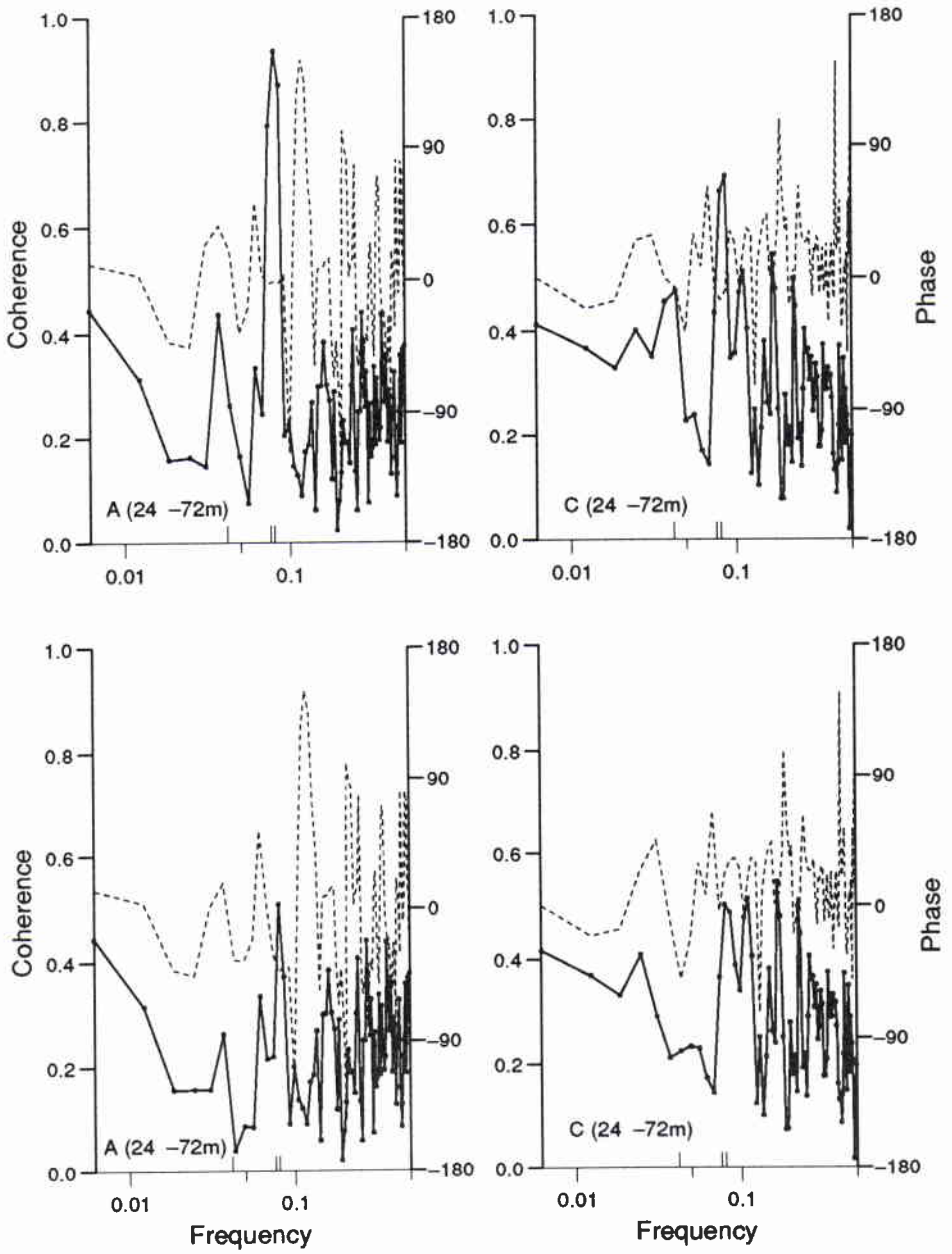

Figure 12b *Rotational coherence spectra (mooring 1991/92), from currents at distant horizons: 24 m vs 72 m. For further explanation see Fig. 11a.*

6

Vertical empirical orthogonal eigenfunctions (EOF)

The method of decomposing the measured vector time series of current velocities into vertical empirical orthogonal eigenfunctions (EOFs) is applied. For this purpose, the two-dimensional current vectors are described by complex numbers as before (3.1). Considering M depth horizons, a $M \times M$ covariance matrix may be estimated by averaging over N time samples:

$$C_{lk} = \frac{1}{N} \sum_n w_{ln} w_{kn}^*, \tag{6.1}$$

where w are zero-mean current velocities, the indices $l, k = 1, \ldots, M$ counting the depth horizons and n the time samples. The EOFs are eigenvectors of the eigenvalue problem

$$\sum_{k=1}^{M} C_{lk} e_k^{(m)} = \lambda^{(m)} e_l^{(m)}, \tag{6.2}$$

where $m = 1, \ldots, M$ are the mode numbers, $e_k^{(m)}$ are mutually orthogonal (complex) eigenfunctions. $\lambda^{(m)}$ are the eigenvalues, which are real because the covariance matrix is Hermitian. The measured time series may be decomposed into EOFs by

$$w_{ln} = \sum_{m=1}^{M} a_n^{(m)} e_l^{(m)}, \qquad \text{with} \quad a_n^{(m)} = \sum_{l=1}^{M} w_{ln} e_l^{(m)}. \tag{6.3}$$

The eigenvalues represent the amount of variance as explained by the respective mode. Normally, a small number of modes contains most of the variance and summation over m in (6.3) may be restricted to values considerably smaller than M. The eigenfunctions contain an arbitrary complex factor.

EOFs are computed from 810 h time series including tides or with the tides S2, M2, N2, K1 and O1 removed. Only depth horizons are considered which are not contaminated by sidelobe reflections. Figures 13a and 13b display the first 3 EOFs as derived from the first and last of 6 partial time series of the 1991/92 mooring. The starting times are indicated in terms of Julian day. It should be noted that the real and imaginary part of the eigenfunctions do not relate to current components, as the EOFs may be arbitrarily rotated by means of the complex normalisation factor. The percentage variance described by the respective EOF is indicated.

EOFs are difficult to interpret as they perform an arbitrary decomposition of the current field which might not relate to oceanic modes. An important shortcoming of our analysis is that the data from the uppermost 15% of the water column cannot be used for the analysis, as they may be contaminated by sidelobe reflections.

Figures 13a and 13b show similar features, to the EOFs from the time series in-between and from the 1990 mooring (not shown here). If tides are present (upper panels), the first EOF contains more than 80% of the variance. There is some variability with depth, which is also present in the M2 tidal ellipses (Fig. 6b and 6c). Removing tides (lower panel), the first EOF loses a considerable percentage of variance and also the depth dependence is modified, but differently for the two time periods analysed. The second and third EOFs are, except of course for the percentage variance, not affected by the removal of tides. These EOFs contain more than 10% of the variance for currents including tides and around 30% after removing the tides S2, M2, N2, K1 and O1.

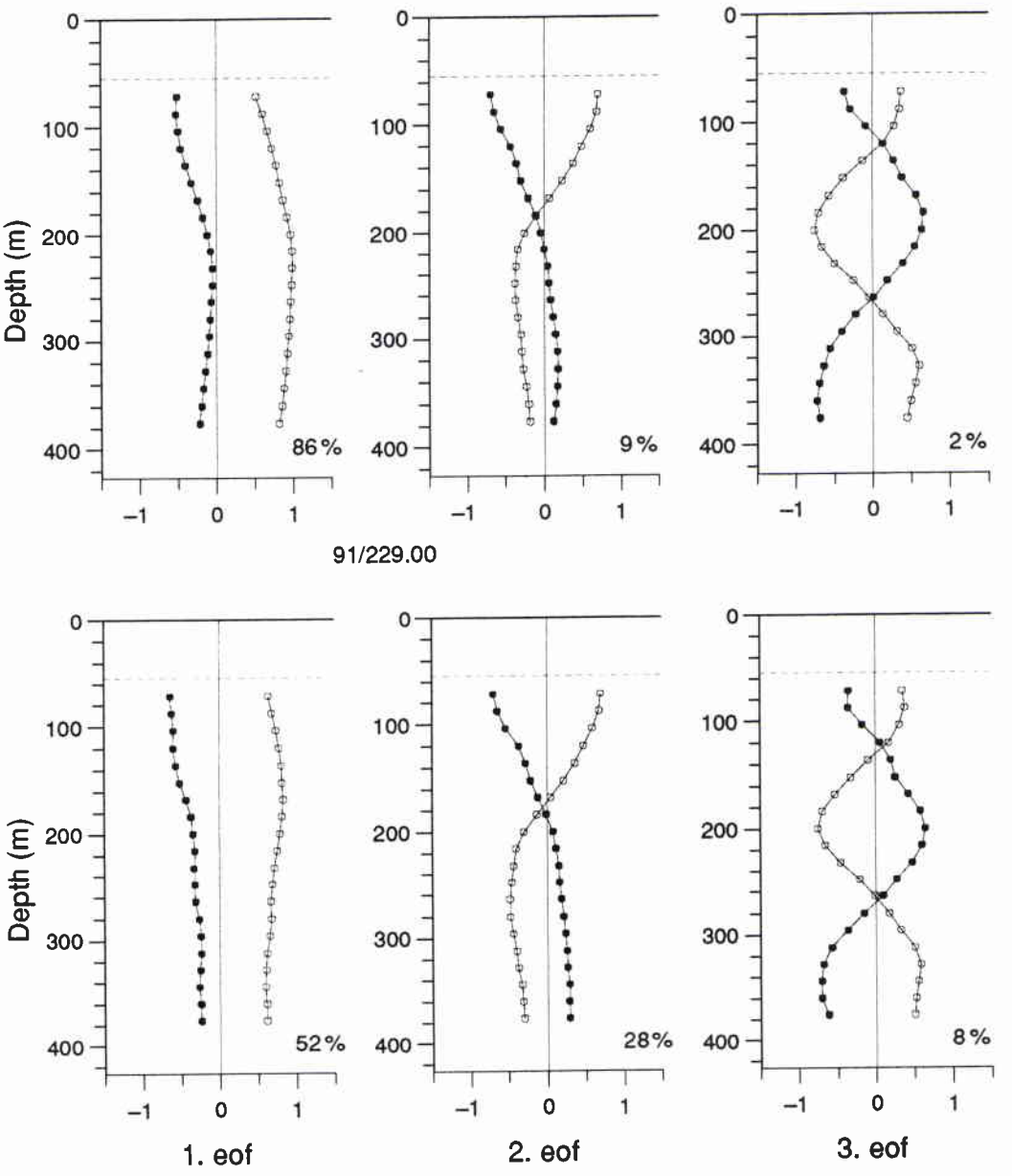

Figure 13a *First 3 vertical EOFs (1991/92 mooring), from first of 6 partial 810 h time series. Currents from below the critical depth for sidelobe contamination (dashed line) are considered only. EOFs are arbitrarily normalised with equal real (open circle) and imaginary part (filled circle) at the uppermost horizon. Upper panel refers to time series containing tides, lower panel to time series with tides S2, M2, N2, K1 and O1 removed. The percentage variance of the single EOFs is indicated.*

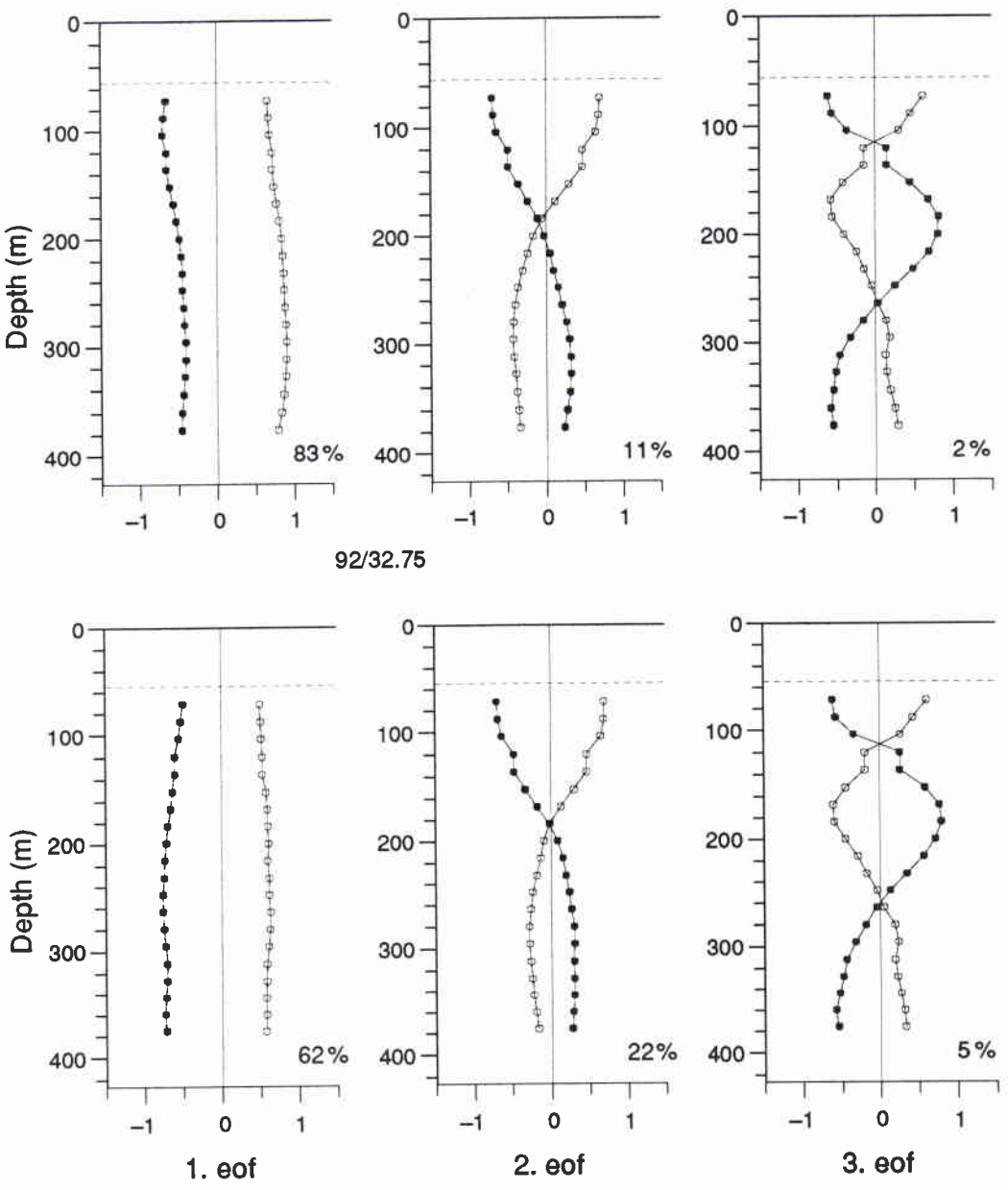

Figure 13b *First 3 vertical EOFs (1991/92 mooring), from last of 6 partial 810 h time series. For further explanation see Fig. 13a.*

7

Correlation of current and wind

Wind data for the period of the half-year mooring of 1991/92 are available from the assimilated wind archive of the UK Meteorological Office, which is produced as part of a global data analysis scheme. The analysis is based on a numerical prediction model using primitive equations. It is on a latitude-longitude grid and has 20 vertical levels. Data assimilation is achieved by the repeated insertion of observational increments. Winds are determined at hourly intervals on a grid with a resolution of 0.833° in latitude and 1.25° in longitude. For the purposes of our analysis, winds are taken from the lowest level of the atmospheric model, being roughly 25 m above sea level. By interpolating to the position of the ADCP, a time series with 6 h sampling has been constructed from these data.

In order to suppress tidal and inertial portions the current time series have been filtered with a running mean of 13 h duration and sampled on the same time grid as the winds. It should be mentioned that this temporal filter is different from that applied to the wind data by the numerical model. As for the analysis in the preceeding sections the total time series is sectioned into 6 parts. The first part is displayed in Fig. 14 comparing winds and currents at the 24 m horizon. Both components of the horizontal velocity vectors and the corresponding stick plot are presented.

The dependence of current on wind is investigated by means of complex correlation analysis. The complex correlation coefficient is defined by

$$R = \rho \exp(i\vartheta) = \frac{1}{\sigma_c \sigma_w} \sum_n w_{cn} w^*_{wn}, \tag{7.1}$$

where w_c and w_w are the zero-mean time series of current and wind, respectively, and $\sigma^2 = \sum_n |w_n|^2$ are the total variances. ρ is a measure of the linear dependence of the two time series involved, ϑ describes the mean veering of the current vector against the wind vector (counting clockwise) and will be discussed later.

Complex correlation coefficients are estimated from the 6 partial time series of the 1991/92 mooring. These series of 810 h duration contain 135 samples. Because of the running mean applied to the current time series, only half of the data can assumed to be statistically independent. In the case of a real correlation coefficient, this would yield the 95% confidence level for zero correlation at $\rho = 0.25$. Complex and real correlation coefficient differ by definition and also the confidence levels may deviate. As no literature on the statistics of the complex correlation coefficient could

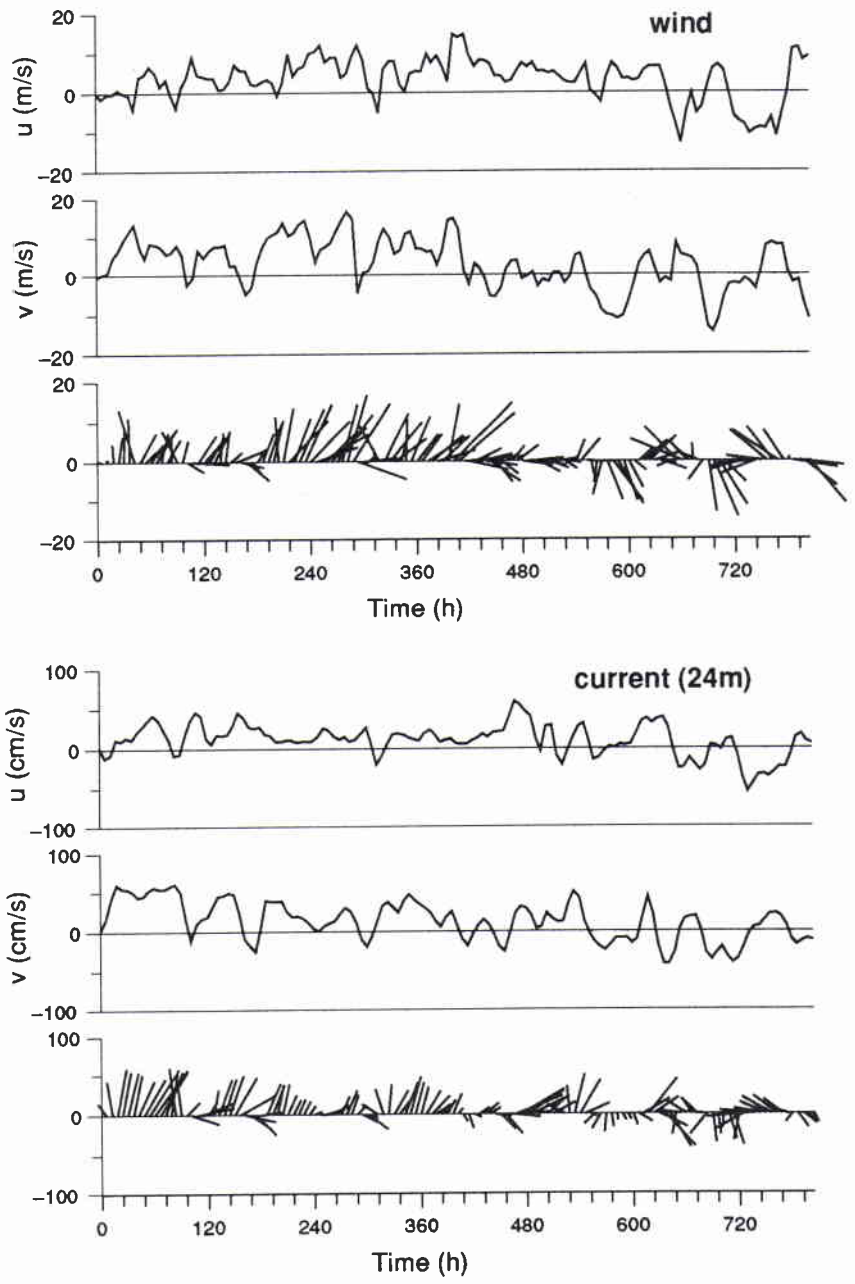

Figure 14 *Comparison of winds and surface currents, from first of 6 partial 810 h time series at 24 m depth. Winds are from the wind archive of the UK Meteorological Office, currents are filtered by a 13 h running mean. East and north component are displayed, and a stick plot with north component upwards, and east component to the right.*

be found, tests with random data have been carried out, confirming the confidence level as given.

Table 4 *Vector correlation between wind and current at different depths, from 810 h time series (starting at the Julian day indicated); the indices refer to the depth horizon of the current data*[1,2,3]

Time	$\rho_{24\,m}$	$\gamma_{24\,m}$	$\vartheta_{24\,m}$	$\rho_{72\,m}$	$\rho_{376\,m}$
91/229.00	0.65	0.025	8.0	0.08	0.26
91/262.75	0.43	0.015	10.2	0.12	0.25
91/296.50	0.63	0.020	4.0	0.13	0.24
91/330.25	0.59	0.016	7.9	0.25	0.11
91/364.00	0.46	0.012	8.1	0.12	0.15
92/ 32.75	0.61	0.013	11.6	0.14	0.11

[1] ρ = absolute value of complex correlation coefficient (7.1).
[2] γ = ratio of current-to-wind speed (7.2).
[3] ϑ[deg] = veering of current against wind (7.2).

Table 4 presents absolute values of the complex correlation coefficients for the six partial time series and currents at different depths, near-surface currents (24 m), the uppermost level of measurements not contaminated by sidelobe reflections (72 m) and the deepest level (376 m). Only the surface currents are significantly correlated with wind.

For further investigating the dependence of current on wind, we introduce a complex regression coefficient

$$r = \gamma \exp(i\vartheta) = \frac{1}{\sigma_w^2} \sum_n w_{cn} w_{wn}^*, \tag{7.2}$$

where γ is the mean ratio of current speed to wind speed and ϑ the same as in (7.1). These values only make sense in the case of significant correlation, and are presented in Table 4 for near-surface currents only. γ yields current speeds between 1.3% and 2.5% of the wind speed which is quite reasonable. The veering ϑ of the current vector against the wind vector is only a few degrees and to the right. The value of veering is smaller than predicted by Ekman's theory but the direction is in accordance with it.

ρ^2 is an estimate of the percentage variance of the current field linearly forced by wind. This is between 18% and 42% for the current at 24 m depth. These values are also quite reasonable. Wind-forcing cannot be considered to be linear and some more variance may be due to wind. In addition, mesoscale processes like eddies are of great importance in the highly variable area around the mooring.

For several reasons the high correlation found is surprising. Wind data are not real but from an analysis scheme, current data of the ADCP are from a depth horizon where measurements may be contaminated by sidelobe reflections and temporal smoothing is performed in different ways for wind and current. The significant correlation, found for all partial time series, thus confirms the assumption that sidelobe reflections are of minor influence at depths just below the surface but also confirms the quality of the analysed wind data.

8
Conclusions

The bottom mounted ADCP is a powerful instrument. It measures horizontal current velocities as function of depth. An important advantage of the ADCP is its vertical coverage, which allows the determination of the barotropic portion of the current field.

From the moorings in the Iceland-Faeroe area some features of the circulation could be determined. Parameters of the barotropic M2 tide have been estimated and found to be highly stable with time. The presence of inertial motions could be established by a broad spectrum around inertial period only for clockwise rotating currents. Except for tides, there is no coherence between currents at the surface and below about $60m$ depth. Only 3 vertical EOFs cover more than 95% of the current's variance, and even about 90% after detrending by tides.

Though near-surface measurements may be contaminated by sidelobe reflections some evidence has been found that suggests the uppermost horizons are not that strongly affected. In general, current measurements from only few metres below the surface cannot easily be obtained. Thus, the ADCP data may help to explain some of the variability as found in other data like temperatures otained from ship surveys just below and satellite images at the sea surface.

References

[1] Carter, G.C., Knapp, C.H., Nuttall, A.H. Statistics of the estimate of the magnitude-coherence function. *IEEE Transactions on Audio and Electroacoustics*, **21**, 1973: 388–389.

[2] Godin, G. The analysis of tides. Liverpool, Liverpool University Press, 1972.

[3] Jenkins, G.M. and Watts, D.G. Spectral analysis and its application. San Francisco, Holden-Day, 1969.

[4] Nuttall, A.H. Spectral estimation by means of overlapped fast fourier transform processing of windowed data. NUSC Report 4169, Naval Underwater Systems Center, 1971.

[5] RD Instruments. Acoustic doppler current profilers, principles of operation. San Diego, RD Instruments, 1989.

Security Classification		Project No.
NATO UNCLASSIFIED		23
Document Serial No.	**Date of Issue**	**Total Pages**
SM-265	December 1992	49 pp.

Author(s)

H.-H. Essen

Title

Ocean currents in the Iceland–Faeroe area, measured by a bottom-mounted ADCP

Abstract

Horizontal currents as a function of depth, measured by a bottom-mounted acoustic doppler current profiler (ADCP) in the Iceland-Faeroe area have been analysed. Because of instrumental limitations it was expected that currents measured in the upper 15% of the water column would be contaminated by side-lobe reflections from the sea surface. Some evidence has been found that this effect is less important in the upper part of the contaminated layer.

The uncontaminated data are of high quality and cover about 75% of the water column. By means of least-squares methods, tidal currents have been extracted. The semidiurnal tide M2 is dominant, its barotropic portion has been estimated from vertically averaged currents. After removing the tides, the only significant variance peak left is for clockwise rotating currents around the inertial period. Vertical coherence between currents at different depth levels has been investigated and a decomposition into empirical orthogonal eigenfunctions (EOFs) has been performed.

A surprisingly high correlation has been found between low-pass filtered current velocities at the (contaminated) near-surface level and wind velocities from the wind archive of the UK Meteorological Office.

Keywords

bottom-mounted ADCP (acoustic doppler current profiler), Iceland-Faeroe area, tides, inertial motions, winddriven currents

Issuing Organization

North Atlantic Treaty Organization
SACLANT Undersea Research Centre
Viale San Bartolomeo 400, 19138 La Spezia, Italy

tel: 0187 540 111
fax: 0187 524 600
telex: 271148 SACENT I

*[From N. America: SACLANTCEN CMR-426
(New York) APO AE 09613]*

Initial Distribution for SM-265

SCNR for SACLANTCEN	
SCNR Belgium	1
SCNR Canada	1
SCNR Denmark	1
SCNR Germany	1
SCNR Greece	1
SCNR Italy	1
SCNR Netherlands	1
SCNR Norway	1
SCNR Portugal	1
SCNR Spain	1
SCNR Turkey	1
SCNR UK	1
SCNR US	2
French Delegate	1
SECGEN Rep. SCNR	1
NAMILCOM Rep. SCNR	1

National Liaison Officers	
NLO Canada	1
NLO Denmark	1
NLO Germany	1
NLO Italy	1
NLO Netherlands	1
NLO UK	1
NLO US	4

Total external distribution	27
SACLANTCEN Library	10
Stock	23
Total number of copies	60